This is to certify that the

thesis entitled

A PHOTOIONIZATION MASS SPECTROMETRIC STUDY

OF ACETONITRILE AND ACETONITRILE-$d_3$

presented by

Gary William Ray

has been accepted towards fulfillment
of the requirements for

Ph.D. degree in Chemical Physics

A. S. Leri
Major professor

Date February 20, 1978

# A PHOTOIONIZATION MASS SPECTROMETRIC STUDY OF ACETONITRILE AND ACETONITRILE-$d_3$

By

Gary William Ray

A DISSERTATION

Submitted to

Michigan State University

in partial fulfillment of the requirements

for the degree of

DOCTOR OF PHILOSOPHY

Department of Chemistry

Chemical Physics Program

1978

G112098

ABSTRACT

A PHOTOIONIZATION MASS SPECTROMETRIC STUDY OF ACETONITRILE AND ACETONITRILE-$d_3$

By

Gary William Ray

Due to its importance as an interstellar molecule and the paucity of vacuum UV spectral data on nitriles, acetonitrile has been studied by means of photoionization mass spectrometry (PIMS). Its deuterated analog, $D_3CCN$, has been included in the study to aid in the data analysis. The photoionization efficiency (P.I.E.) curves from threshold to 600 Å of $H_3CCN^+$, $H_2CCN^+$, $HCCN^+$, $CH_2^+$, $CH_3^+$ and $D_3CCN^+$ resulting from the photoionization of acetonitrile and acetonitrile-$d_3$ have been determined for the first time. Their appearance potentials have been determined and also those of $D_2CCN^+$, $DCCN^+$, $CD_2^+$ and $CD_3^+$. The appearance potentials of the deuterated ions as well as that of $CH_3^+$ have not been reported heretofore. An autoionizing Rydberg series has been observed in the P.I.E. curves of $H_3CCN^+$ and $D_3CCN^+$ and assigned to an ns$\sigma$ series converging to the $\tilde{A}^2A_1$ excited state of the parent ion. All of the fragment ions studied have appearance potentials that lie between the thresholds of the $\tilde{A}^2A_1$ and $\tilde{B}^2E$ state of the parent ions.

At lower energies they appear to be formed by the predissociation of autoionizing Rydberg states. However, after the energy of the exciting light has reached the threshold of the $\bar{B}^2E$ state of the parent ion the fragment ion P.I.E. curves rise sharply, indicating that most of their intensity is the result of the predissociation of this state. Finally, the appearance potentials reported here have been used to derive several thermodynamic parameters.

This dissertation is dedicated to my parents, who got me started, and to my wife, who helped me finish the task. May my efforts be worthy of theirs.

## ACKNOWLEDGMENTS

I would like to thank my advisor, Professor George E. Leroi, for his friendship, patience, guidance and encouragement during the course of my studies. His efforts will long be remembered. I would also like to thank my second reader, Professor Paul M. Parker, for his many helpful suggestions during the writing of this dissertation.

I am especially grateful to Dr. Edward Darland, who designed the lion's share of the MSU PIMS apparatus, and to Mr. David Rider, whose help was so vital during the final stages of my experiments. I would also like to thank Dr. Darland for allowing me to use his drawing of the apparatus in Figure II-1.

My gratitude also goes to the many members of the Molecular Spectroscopy Group for their friendship over the years. Special thanks go to Mrs. Naomi Hack for her interesting discussions and willingness to do a "quick typing job" at a moment's notice.

The financial support of the Office of Naval Research and the NSF is gratefully acknowledged.

# TABLE OF CONTENTS

LIST OF TABLES

## LIST OF FIGURES

# CHAPTER I

## INTRODUCTION

The presence of several molecular species in the galactic environment (e.g., interstellar nebulae and stellar atmospheres) has been known for some time.[1] As detection techniques have improved, more molecules of increasing complexity have been discovered. Recent theoretical and laboratory work has interpreted a newly discovered set of radio frequency spectral lines as belonging to a molecule with an eleven carbon backbone. These discoveries have naturally led to many investigations into the nature of interstellar chemistry.[2] The energy source for interstellar chemical reactions is still not well understood. At the average temperature of interstellar nebulae (about 100°K) most neutral-neutral reactions are inhibited as their potential energy surface barrier heights exceed the available thermal energy. Moreover, photodissociation and photoionization must be ruled out as the available ultraviolet light from nearby stars is heavily attenuated by the material of the dense (about $10^8$ particles/$cm^3$) nebulae in which the more complex molecules have been discovered.[3] Recently, a new quantitative theory of interstellar chemistry has been developed by Herbst and Klemperer.[4] They suggest that the driving force of interstellar chemistry is ionization by cosmic rays. A substantial cosmic ray flux is provided by stars nearby to or imbedded in the interstellar nebulae. Significantly, this flux is not attenuated by the nebular material. Since the initial step in this model is ionization by cosmic rays, one would expect interstellar chemistry to be predominantly ion-molecule reactions with the rare exception of a neutral-neutral reaction of low activation energy. Herbst and Klemperer have shown that their model can account for most of the molecules so far discovered in interstellar space. In order for the theory to receive a quantitative test, the thermodynamic parameters (e.g., heats of formation, bond dissociation energies, electron and proton affinities) associated with each ion and molecule in a given ion-molecule reaction must be known. The technique of photoionization mass spectrometry (PIMS) is one of the best and most widely used methods employed to determine such parameters.

It is not my intention here to provide more than a brief review of PIMS, since there are several fine, though somewhat dated, reviews available.[5,6] However, I wish to provide enough basic information to allow the reader to follow this dissertation without undue effort. As is well known, the mass spectrum of any molecule is comprised of the molecular (parent) ion and several fragment ions - provided that the energy of the ionizing radiation is sufficiently large. In order to derive the aforementioned thermodynamic quantities, it is necessary to measure the energy thresholds for the formation of the parent ion and each of its fragment ions. This requires a mass spectrometer that is capable of accurately measuring the energy dependence of the cross section for the formation of each of the ions. This has often been accomplished with an instrument equipped with an electron bombardment source whose voltage can be accurately varied. A photoionization mass spectrometer performs the same task with improved energy resolution with a continuum source of vacuum ultraviolet radiation and a vacuum monochromator. The photoionization cross section, $\sigma_i$, is defined as the number of ions produced per absorbed photon or

$$\sigma_i \equiv \sigma N_i/(I_0 - I), \qquad (1)$$

where $\sigma$ is the absorption cross section, $N_i$ is the number of ions produced per second, $I_0$ is the incident photon intensity and I is the transmitted photon intensity.[7] Actually, a PIMS instrument is incapable of measuring $\sigma_i$ since vacuum monochromators are only single beam instruments. In addition, the difference between $I_0$ and I would be very difficult to measure anyway as the absorption cross sections in the vacuum ultraviolet region are very small ($10^{-18}$ cm$^2$ or less). Consequently, a quantity called the photoionization efficiency is measured for each ion as a function of wavelength or energy. The photoionization efficiency (P.I.E.) is defined as the number of ions formed per transmitted photon or

$$\text{P.I.E.} \equiv N_i/I. \qquad (2)$$

It has been shown that for sufficiently low pressures (where $I/I_0$ is at least 90%) the ratio of the P.I.E. to $\sigma_i$ is nearly unity.[8] A PIMS instrument is somewhat less useful for routine structural, qualitative and quantitative analysis than its electron bombardment counterpart due to the relatively low intensity of most sources of vacuum ultraviolet continua. However, the use of photoionization gives this technique two distinct advantages over conventional instruments in the type of study of interest here.

First, as mentioned earlier, thermodynamic data on a molecule and its photofragments (both charged and neutral) may be derived if the energies at which a molecule's fragment ions appear are known. The derivation of such quantities will be discussed in more detail later. Obviously, the more accurately one determines these thresholds, the more accurate will be the resulting thermodynamic quantities. Under favorable conditions, the energy resolution in a PIMS experiment may be as high as 0.001 eV due to the wavelength resolution available from vacuum monochromators. This is two orders of magnitude better than the best results attainable with an electron bombardment mass spectrometer, since the resolution of electron bombardment sources is always limited by the kinetic energy distribution of the electrons leaving the heated filament.

A second advantage of PIMS is that the thresholds for direct photoionization and ionic fragmentation are much easier to observe than in the case of electron bombardment. It has been shown that the cross section for direct ionization is related to the energy of the ionizing radiation in the following way:

$$\sigma_i \propto E^{n-1} \qquad (3)$$

where n is the number of electrons leaving the collision complex.[9] The cross section for ionization by electron impact thus displays a linear, slowly rising dependence on the electron energy, because two electrons leave the collision complex. The onset of ionization is often difficult to observe, because the cross section is nearly zero at threshold. However, the cross section for photoionization is constant and has a finite value at threshold (i.e., it is a step function). This makes the direct photoionization threshold relatively easy to observe. The thresholds for higher energy processes (transitions to excited vibrational and electronic states of the ion) are then superimposed upon the constant direct ionization cross section (P.I.E.). However, other factors may intervene that complicate this obviously ideal case. Since photoionization is a vertical process, the relative intensities of the observed transitions are controlled by their Franck-Condon factors. In those favorable cases where the ionic ground state geometry does not differ significantly from that of the neutral molecule, one of the vertical transitions will also be the adiabatic transition. The adiabatic transition is between the ground electronic, vibrational and rotational state of the neutral molecule and the ground electronic, vibrational and rotational state of the ion. However, in some cases the Franck-Condon factor for this transition may be so small that it is observed as an exceedingly weak step or is totally absent from the P.I.E.[10]

A further complication may occur when neutral molecules in excited rotational or vibrational states are photoionized. The result is usually weak structure (hot bands) below the energy of the true vertical transition from the molecular ground state. Rotational hot bands are usually diffuse and structureless as the rotational levels are too closely spaced to be resolved by most PIMS instruments. Vibrational hot bands often appear as fairly well defined steps. Either type of hot band masks the position of the actual threshold. Cooling the sample will, in most cases, remove such structure.

As mentioned previously, the thresholds for transitions to excited states of the ion will be superimposed on the P.I.E. curve for ionization to the ionic ground state at energies above the first ionization potential. However, these thresholds are often obscured by additional structure that is also superimposed on the P.I.E. curve. In addition to its valence electronic levels, every molecule displays many sets of Rydberg levels at higher energies.[11] As in the case of hydrogen, some of the Rydberg levels occur in series that converge to the first ionization potential of the molecule. However, in the cases of molecules and many-electron atoms, other series converge to excited states of the ion as well. Necessarily, some of these Rydberg states occur at energies above that of the first ionization potential and are imbedded in the first ionization continuum, and the corresponding wavefunctions are actually mixed Rydberg and continuum wavefunctions.[12] Thus, electrons excited to these neutral molecule states may "cross over" to the continuum and leave the molecule. When this occurs, "autoionization" structure will appear on the P.I.E. curve. This structure is not observed in those cases where predissociation of the Rydberg states (leading to neutral fragments) depopulates them faster than the autoionization rate.

Fragment ions are formed when the energy of the ionizing photons exceeds the first ionization potential sufficiently to cause dissociation of the parent ion.[13] If we photoionize a molecule AB, where A and B are atoms or groups of atoms, two fragment ion forming processes may be observed, dissociative ionization

$$AB + h\nu = A^+ + B + e^- \qquad (4)$$

and ion pair formation

$$AB + h\nu = A^+ + B^-. \qquad (5)$$

Generally, fragment ions are formed by the ionization and excitation of a molecule to an excited ionic state or to an autoionizing Rydberg state followed by predissociation.[14] In some cases, the state of the parent molecular ion reached by photoionization may have a repulsive potential surface. Either situation precludes the observation of step-function like onsets for fragment ion formation. Hot rotational bands may also serve to mask the threshold further. Kinetic factors may be at work here as well. Most ionic fragmentation processes have a minimum "activation energy" that must be exceeded. This is termed the "kinetic shift". The presence of the kinetic shift will cause the measured fragmentation threshold to be higher than the true thermodynamic value. These factors often prevent precise determination of ionic fragmentation thresholds. Consequently, the values reported are termed "appearance potentials". If the kinetic shift is not large, the appearance potentials can be reported with known limits of accuracy. If the kinetic shift is large, the accuracy of a reported value may be questionable and will at best be an upper bound to the actual value.

Once the ionization potential and fragment ion appearance potentials of a molecule have been determined, the values may be incorporated in thermodynamic cycle calculations (along with other data) to derive thermodynamic quantities of interest. As an example, let us consider the dissociative ionization of our general molecule AB:

$$AB + h\nu = A^{+} + B + e^{-}. \tag{6}$$

The appearance potential of $A^+$ ($AP(A^+)$) corresponds to the heat of reaction for this endoergic process. When the appearance potential is corrected to its 0°K value, we may write

$$AP(A^{+}) = \Delta H_f(A^{+}) + \Delta H_f(B) - \Delta H_F(AB), \tag{7}$$

since $\Delta H_f = \Delta G_f$ at that temperature. If any two of the heats of formation are known, the third can be determined. In addition, since

$$\Delta H_f(A^{+}) = \Delta H_f(A) + IP(A), \tag{8}$$

where IP(A) is the ionization potential of the fragment A, Equation (7) becomes

$$AP(A^+) = \Delta H_f(A) + IP(A) + \Delta H_f(B) - \Delta H_f(AB) \qquad (9)$$

or

$$AP(A^+) = IP(A) + D_0(A\text{-}B) \qquad (10)$$

where $D_0(A\text{-}B)$ is the energy of the A-B bond. Other quantities may be derived depending upon the data obtained and the thermodynamic data available in the literature.

Acetonitrile was chosen as the subject for this investigation for several reasons. It has been discovered in interstellar nebulae. It provides an interesting problem in mass spectrometry (as will be seen in Chapter III). In addition, very few data exist in the literature on nitriles despite the fact that they are an important class of compounds.[15]

## CHAPTER II

## EXPERIMENTAL

### A. The Instrument

The Michigan State University PIMS apparatus and its associated data acquisition equipment have already been described in great detail.[16] A general description of the instrument is sufficient for the purposes of this dissertation. During this discussion the reader should refer to the diagram of the MSU PIMS instrument in Figure II-1.

Vacuum ultraviolet radiation is produced by a Hinter-regger-type discharge lamp (LP). For the experiments described here, the well known Hopfield continuum of He and pseudo-continuum of $H_2$ were employed. They were excited by high voltage pulsed D.C. and high voltage D.C. discharges, respectively. The Hopfield continuum provides usable light intensity in the region from about 600 Å to 1000 Å. The $H_2$ pseudo-continuum provides usable intensity from about 930 Å to 1800 Å. For the purposes of obtaining mass spectra, a D.C. discharge through low pressure He (about 1 torr) was used to produce the intense HeI atomic resonance line (584.32 Å or 21.218 eV). As the lamp must be operated in a windowless configuration, two stages of

BA Baffle

EN Entrance Slit

EX Exit Slit

GR Grating

IS Ion Source

IT Ion Transducer

LP Lamp

P1 First Differential Pumping Port

P2 Second Differential Pumping Port

P3 Monochromator Pumping Port

P4 Sample Chamber Pumping Port

P5 Quadrupole Chamber Pumping Port

PT Photon Transducer

QP Quadrupole Mass Filter

QS Quadrupole Support

Figure II-1. Location of components within the vacuum chambers.

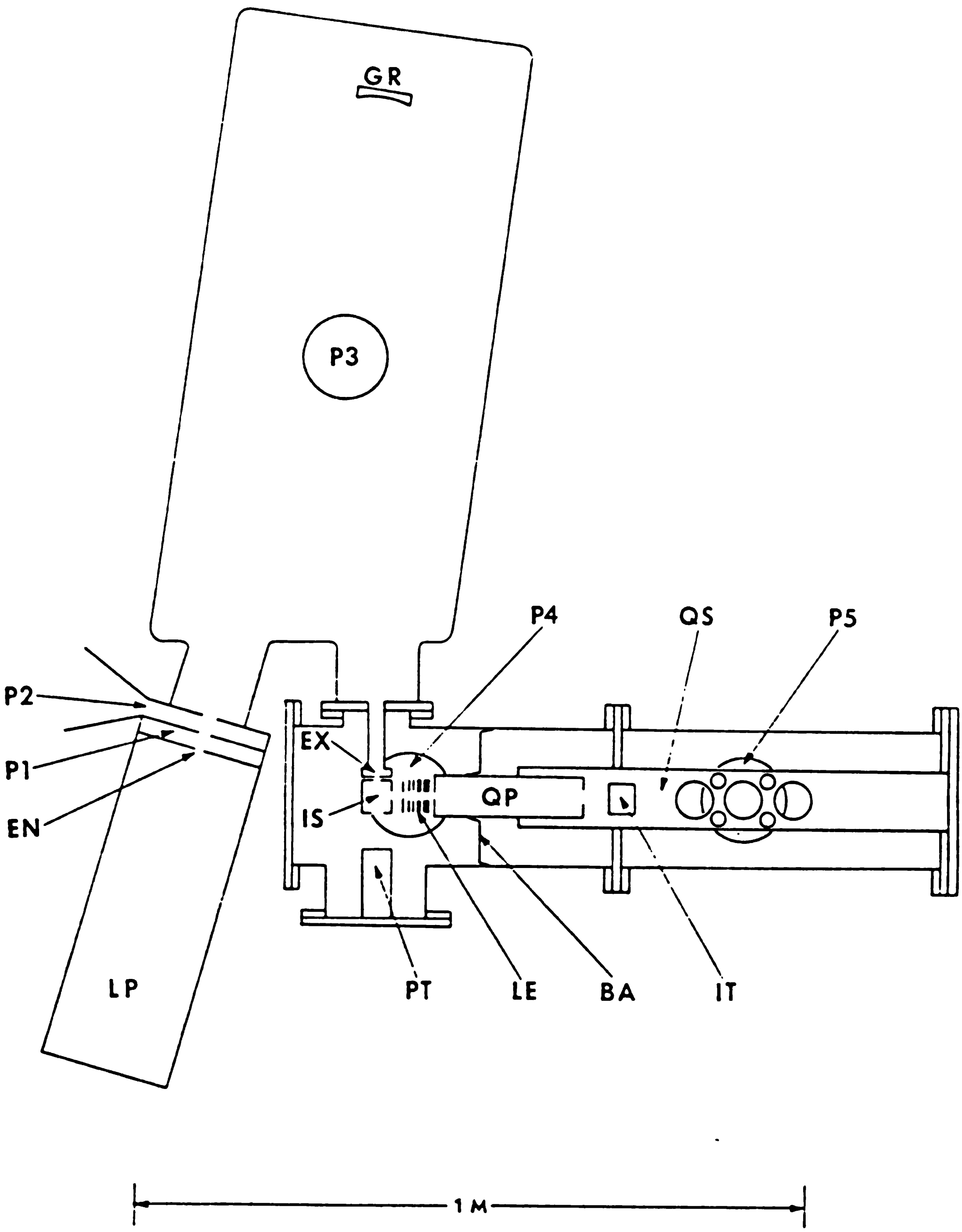
GR
P3
P2
P1
EN
EX
IS
P4
QS
P5
QP
LP
PT
LE
BA
IT
1 M

differential pumping are provided. Pump P1 is a 300 l/sec Roots-type blower and P2 is a 300 l/sec four inch diffusion ejector pump.

The radiation from the lamp is dispersed by a McPherson 225 one-meter near-normal-incidence monochromator. The concave diffraction grating (GR) is aluminum coated with a $MgF_2$ overcoating, blazed at 1200 Å and ruled with 1200 lines/mm. It provides a reciprocal linear dispersion of 8.3 Å/mm. With 100 micron entrance and exit slits (as used in most of these experiments) it provides a resolution of approximately 0.83 Å or 0.010 eV at 1000 Å. Three different entrance slits (EN) are mounted on a disk that is rotatable from outside of the apparatus by means of a vacuum tight feedthrough. Similarly, one of four exit slits (EX) may be chosen by means of a hand operated sprocket-and-chain drive that actuates a rack and pinion. The exit slits are mounted on the vertical rack and are moved up or down by means of a knurled knob outside of the vacuum chamber that is connected to the main drive sprocket. The monochromator is evacuated by an 1800 l/sec six inch oil diffusion pump, P3.

The light emerging from the exit slit passes through the ion source (IS). A drawing of the ion source appears in Figure II-2. It is basically a simple ambient temperature ion source machined from 311 stainless steel and mounted on the exit slit holder which is electrically

Figure II-2. Schematic diagram of the ion source.

RP = Repeller Plate

R = Repeller Radius of Curvature

CS = Ceramic Standoff

GI = Gas Inlet

IE = Ion Exit

EL = Electrostatic Lens

EnS = Entrance Slit

ExS = Exit Slit

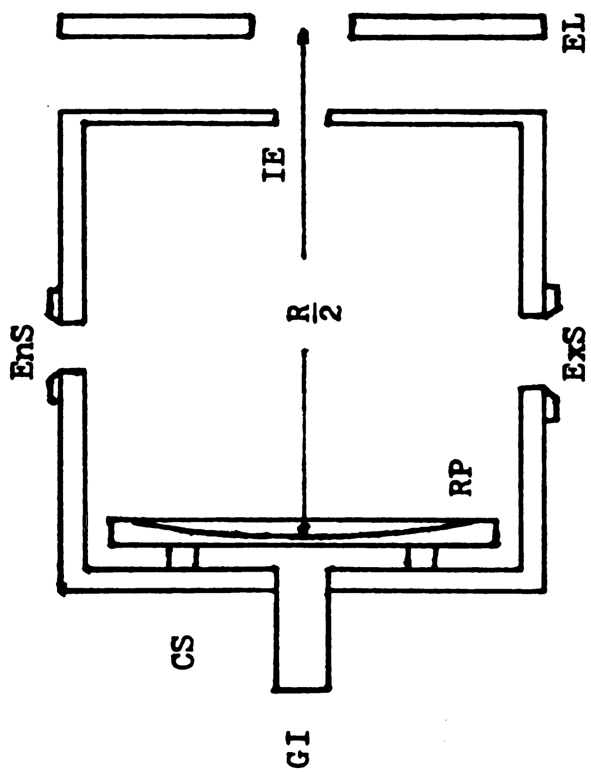
EL
IE
R/2
EnS
ExS
RP
CS
GI

insulated from the rest of the monochromator. The ion source is fitted with entrance and exit slits that are wide enough to allow the uninhibited passage of the light beam. For future experiments, the exit slit should be made narrower to allow for higher sample pressures while maintaining a low background pressure in the vacuum chamber. Of course, photoelectrons would be produced by the light striking the interior of the ion source. However, these can be trapped by placing a small metal plate, electrically insulated from the rest of the ion source, below the entrance slit. A small positive potential on the plate will attract the unwanted photoelectrons.

Ions formed in the ion source exit through a circular aperture transverse to the light beam. The diameter of the aperture may be varied and is covered with a fine gold coated mesh (90% transmissivity) to insure a uniform potential within the source itself. The ions are pushed out of the ion source by a positive potential placed on the repeller. In most PIMS instruments the repeller is a simple flat plate that is electrically insulated from the rest of the ion source. One PIMS research group has designed a focused repeller, which consists of a metal plate bent into a modified U-shape.[17] However, this did not provide effective focusing of the ions as the repeller voltage could be varied by ±0.5 volts without any change in the measured ion intensity.[18] In view of the many analogies between charged particle and physical optics, our repeller has been fashioned in the shape of a spherical mirror. The repeller is a 311 stainless steel plate with a spherical depression machined into one face. The focal point of a spherical mirror is on a normal to the mirror's surface at a distance of R/2, where R is the mirror's radius of curvature. Consequently, the radius of curvature of our repeller is twice the distance from the repeller to the first element of the mass filter lens system. This seems to provide a closer approximation to a truly focused system as a variation of ±0.1 volts or less will cause a significant change in the measured ion intensity.

Sample gases are introduced by means of a stainless steel tube entering behind the repeller. An identical tube leads out of the ion source, transversely to the inlet tube, to a capacitance manometer that monitors the sample pressure.

After passing through the ion source, the transmitted photons are detected by the photon transducer (PT). For these experiments, the transducer is a sodium salicylate phosphor - RCA 8850 photomultiplier system. The vacuum ultraviolet radiation is absorbed by a thin layer of sodium salicylate deposited on a quartz disc. The excited phosphor in turn fluoresces in a wide band whose peak intensity occurs at approximately 4200 Å. The fluorescence is conducted down a Lucite light pipe that joins the quartz disc to an RCA 8850 photomultiplier in a Pacific Photometrics thermoelectrically cooled housing. The advantage of such a system is that sodium salicylate has a nearly constant quantum yield from around 200 Å to 1200 Å.[19] Since the photomultiplier tube is always presented with light of the same wavelength, there results a detection system whose sensitivity as a function of wavelength is constant. This is in marked contrast to the other detectors that are often used, such as bare photomultipliers, electron multipliers and simple photocathodes whose sensitivity varies considerably with wavelength. Accordingly, they must be calibrated with the sodium salicylate phosphor-photomultiplier detection system. However, the latter system has its shortcomings as well. It is sensitive to the near ultraviolet and visible light that is produced by our lamp, which is scattered, undiffracted, off the grating. This produces a large background photon signal. Moreover, photomultipliers are much noisier than electron multipliers. Perhaps the two greatest shortcomings are that the sodium salicylate is often chemically degraded by a significant number of compounds and it is slowly aged by contamination by diffusion pump oil vapors. The scattered light effects may be corrected for during post-experiment data analysis. Photomultiplier noise is considerably reduced when the multiplier is cooled. Moreover, the relatively weak ion signals require long counting times that improve the photon signal-to-noise ratio even further. When reactive gases are in use, electron multipliers and bare metal photocathodes must be used. Frequent changing of the sodium salicylate phosphor will prevent aging effects from altering the data.

Ion focusing and mass analysis are performed by an Extranuclear quadrupole (QP) mass filter and its associated electrostatic lenses (LE). The ion transducer (IT) is a Johnston Laboratories MM-1 focused mesh electron multiplier.

The vacuum chamber that houses the ion source, ion optics, quadrupole mass filter and photon and ion transducers is pumped by two six inch oil diffusion pumps, P4 and P5. All of the oil diffusion pumps on the apparatus are trapped by freon refrigerated baffles in order to reduce backstreaming of the pump oil into the vacuum chamber. The Roots-type blower, mechanical backing pumps and refrigeration units are housed in a small room in one corner of the laboratory in order to minimize the amount of noise and heat in the main room. All of the pump exhaust ports are connected to a fume hood to keep pump oil vapors and toxic gases out of the laboratory.

Sample gases are fed into the ion source by means of a variable leak valve that is incorporated into a metal vacuum manifold. One half of the manifold, for chemically inert gases, is constructed from copper tubing and brass valves while the remainder is constructed entirely from stainless steel in order to handle more corrosive species. The substitution of brass and copper for stainless steel wherever possible has resulted in a considerable savings on the construction cost of the manifold.

The MSU PIMS instrument is interfaced to a Digital Equipment Corporation PDP-8/M minicomputer. Signals from the photon and ion transducers are amplified by a Keithley 427 current amplifier and a Keithley 417 high speed picoammeter, respectively. The output signals of the amplifiers are fed to voltage-to-frequency converters and the converter signals are interfaced into the computer. Once the initial instrumental operating parameters are set, the entire experiment is automated with the computer in control of all aspects of data acquisition. The computer changes the wavelength setting by an amount chosen by the user through a stepping motor attached to the monochromator drive screw. At the beginning and end of each experiment, measurements are taken to estimate the scattered light contribution to the photon and ion signals. Throughout the experiment, measurements of the dark currents of the detectors are taken at prespecified intervals. In addition, reference measurements at a prespecified wavelength are taken throughout the experiment to monitor drifts in lamp intensity, sample pressure and the detectors. In order for the operator to judge the quality of the data during the actual experiment, a P.I.E. curve approximately corrected for stray light and detector dark current drift is generated in real time.

A unique aspect of the data acquisition capabilities of the MSU instrument is the ability to achieve a constant signal to noise ratio throughout an experiment. This is accomplished by a variable counting time option in the operating program of the computer. The user specifies the minimum number of ion counts for the computer to accumulate and minimum and maximum counting time limits. At each data point the computer counts for the minimum specified time and then computes the ion count rate. If the minimum specified number of counts has been accumulated, the P.I.E. (ions per sec/photons per sec) will be computed, logged and plotted and the computer will step the monochromator to the wavelength of the next datum. If the minimum count has not been accumulated, but the computed count rate indicates that it will be reached within the maximum allowed counting time, the computer will continue to count for the time required to reach the minimum count. If neither of the above is achieved, the computer will plot the P.I.E. for that datum and move to the next wavelength. Such a procedure provides the advantage of minimizing the duration of each experimental run by counting only as long as necessary to achieve the desired signal-to-noise ratio. This is important as PIMS experiments are typically long (as much as 60+ hours) due to the often very low ion count rate (sometimes as low as 1 count per sec or less).

## B. Samples

Acetonitrile (99% purity) and acetonitrile-$d_3$ (99 atom % purity) were obtained from the Aldrich Chemical Company. Although these purities are quite sufficient for most PIMS studies, further purification was undertaken in order to remove dissolved air from the samples.

The sample containers were spherical pyrex vessels of approximately 0.5 liters in volume. Samples were introduced through a 0.5 inch O.D. glass-to-metal transition tube. A 0.25 inch O.D. glass-to-metal transition tube leads to the sample inlet manifold by way of a polyethylene tube. The tube is connected to the manifold and vessel by means of Cajon "Ultra-torr" unions. Similarly, the 0.5 inch O.D. sample introduction tube is sealed off by means of an appropriate union with one end blocked off by a stainless steel rod. Before the samples are placed in a vessel, it is pumped down to approximately $6 \times 10^{-7}$ torr by the sample-mass spectrometer chamber diffusion pumps for one hour. The samples are then subjected to three freeze-pump-thaw purification cycles at dry ice temperature (-78.5°C) until they could be pumped down to $6 \times 10^{-7}$ torr or less while frozen.

## C. Experimental Procedure

As mentioned previously, mass spectra of acetonitrile and acetonitrile-$d_3$ were taken using the HeI 584 Å line. The intensity of this line is comparable to that of the Hopfield continuum when viewed at central image. Since the HeI line is positioned near the high energy end of the Hopfield continuum (600 Å), one is able to measure the relative intensities of all of the ions created from a given parent compound at energies between 21 eV and threshold. Mass spectra were taken at several pressures on the order of one mtorr (micron) to determine the pressure dependence of the ion intensities (see Chapter III-A). The ion optics were adjusted in order to maximize the measured ion intensities (this matter is treated in more detail in Chapter III-A). The quadrupole mass filter was adjusted to provide mass resolution sufficient to cause the ion current to go to zero between adjacent peaks in the mass spectrum. The ion transducer (Johnston MM-1 electron multiplier) voltage was kept at 3.0 kV. Higher voltages increased the intensity of the ion signals with an equivalent increase in the noise and background signals. For this reason, they were not used. The mass spectra were measured by hand-tuning the mass control on the mass filter control unit while observing the ion intensities indicated on the picoammeter voltmeter. The very weak signals ($10^{-12}$ to $10^{-11}$ amps) of some of the ions were extremely noisy.

Since these signals were not integrated, the reliability of their absolute values is questionable - probably no better than ±25%.

The photoionization efficiency curves were measured using the He Hopfield continuum for the 600 Å to 950 Å region, while the $H_2$ pseudo-continuum was used from 930 Å to 1030 Å where the intensity of the Hopfield continuum becomes comparable to that of the scattered light. The sample pressures were kept around 0.6 mtorr. The voltage on the photon transducer (RCA 8850) was adjusted to maximize the multiplier current with a minimum of noise (typically 1.2 kV). All other instrumental operating parameters were identical with those used in obtaining the mass spectra.

It is difficult to accurately determine the average signal-to-noise ratio for these experiments as the output frequency of the voltage-to-frequency converters is proportional to the current amplifier (picoammeter) output voltage - not to the actual ion count rate. A high speed pulse counter was available for some of the preliminary experiments. However, a malfunction caused it to be unusable for the bulk of this work. A comparison between a picoammeter and the pulse counter indicated that an ion current of $3 \times 10^{-11}$ amps corresponded approximately to a count rate of 100 ions/sec. Using this count rate as a standard, integration times were set (see Chapter II-A) to achieve a signal-to-noise ratio of approximately 100:1 provided that all of the observed noise was random. However, it was not possible to achieve such a high signal-to-noise ratio with the lower intensity ions without resorting to unreasonable integration times ($10^4$ sec/datum at a count rate of 1 ion/sec). In such cases, the entire experiment was carried out at the longest possible integration time available in the current operating program which is 405 seconds.

# CHAPTER III

# RESULTS AND DISCUSSION

## A. The Mass Spectrum

The mass spectrum of acetonitrile is surprisingly rich for a molecule comprised of only six atoms. Franklin, Wada, Natalis and Heirl reported the mass spectrum along with a study of the ion-molecule reactions between the acetonitrile molecular ion and the neutral molecule.[20] They reported thirteen primary ion mass peaks and three ion-molecule reaction products for $H_3CCN$ and eleven primary ion mass peaks and four ion-molecule reaction products for $D_3CCN$. Unfortunately, the energy of their ionizing electron beam is not clearly stated. If their earlier works are any indication, it was probably in excess of 30 eV. Table III-1. presents mass spectra for $H_3CCN$ and $D_3CCN$ taken on the MSU PIMS apparatus. The ionizing radiation in this case was provided by the HeI resonance line (584.334 Å, 21.218 eV). The ion source pressure was 0.2 mtorr and the repeller voltage was set at +10 V with respect to the ion source potential in order to minimize the time spent in the ion source by the primary ions. With the exception of the ions m/e = 24 and m/e = 25, we have observed the same ions with similar relative intensities

Table III-1. Acetonitrile and acetonitrile-$d_3$ photoionization mass spectra. Ionizing energy = 21.21 eV; sample pressure = 0.20 mtorr; repeller voltage = +10 V

| m/e | Intensity Relative to $CH_3CN^+$ (m/e=41) | Possible Formula | Intensity Relative to $CD_3CN^+$ (m/e=44) | Possible Formula |
|---|---|---|---|---|
| 12 | trace | $C^+$ | trace | $C^+$ |
| 13 | 0.018 | $CH^+$ | ----- | ---- |
| 14 | 0.096 | $CH_2^+$ | 0.004 | $CD^+$ |
| 15 | 0.035 | $CH_3^+$ | ----- | ---- |
| 16 | ----- | ---- | 0.11 | $CD_2^+$ |
| 18 | ----- | ---- | 0.051 | $CD_3^+$ |
| 26 | 0.020 | $CN^+, C_2H_2^+$ | 0.002 | $CN^+, C_2D^+$ |
| 27 | 0.019 | $HCN^+, C_2H_3^+$ | ----- | ---- |
| 28 | 0.34 | $N_2^+, H_2CN^+$ | 0.52 | $N_2^+, C_2D_2^+, DCN^+$ |
| 30 | ----- | ---- | 0.010 | $D_2CN^+, C_2D_3^+$ |
| 32 | 0.19 | $O_2^+$ | 0.14 | $O_2^+$ |
| 38 | 0.021 | $C_2N^+$ | 0.007 | $C_2N^+$ |
| 39 | 0.10 | $HC_2N^+$ | ----- | ---- |
| 40 | 0.89 | $H_2C_2N^+$ | 0.18 | $DC_2N^+$ |
| 41 | 1.0 | $H_3C_2N^+$ | ----- | ---- |
| 42 | 0.12 | $H_4C_2N^+$ | 0.91 | $D_2C_2N^+$ |

Table III-1. Continued.

| m/e | Intensity Relative to $CH_3CN^+$ (m/e=41) | Possible Formula | Intensity Relative to $CD_3CN^+$ (m/e=44) | Possible Formula |
|---|---|---|---|---|
| 44 | ----- | ---- | 1.0 | $D_3C_2N^+$ |
| 46 | ----- | ---- | 0.086 | $D_4C_2N^+$ |
| 53 | 0.019 | $H_3C_3N^+$ | ----- | ---- |
| 54 | 0.05 | $H_4C_3N^+$ | 0.002 | $D_2C_3N^+$ |
| 56 | ----- | ---- | trace | $D_3C_3N^+$ |
| 58 | ----- | ---- | 0.004 | $D_4C_3N^+$ |

as Franklin and coworkers. Differences are bound to exist due to the use of different ionizing energies, source pressures and mass spectrometers. Of course, the question arises as to why the m/e = 24 and m/e = 25 peaks were not observed in the present study. This question may be answered by comparing the appearance potentials of these ions to the energy of our radiation source. Table III-2 lists the m/e peaks observed by Franklin and coworkers along with their possible formulae. With the choices of the neutral fragments listed in the third column, zero-degree Kelvin appearance potentials have been calculated for each ion from the latest thermodynamic data in the literature.[21] Appearance potentials were not calculated for the deuterated ions as their values should be very similar to those of the protonated species. For the m/e = 24 ion, assumed to be $C_2^+$, four appearance potentials are possible. If the neutral fragments are N + $H_2$ + H, $NH_2$ + H or NH + $H_2$, the calculated appearance potentials are 26.8 eV, 23.6 eV, and 23.1 eV, respectively. These are all clearly above the energy of the HeI resonance line. The other calculated value is 19.3 eV, assuming that the neutral fragment is $NH_3$. Thus it would appear that the absence of $C_2^+$ (m/e = 24) from the photoionization mass spectrum is due to its relatively high appearance potential. A similar situation exists for m/e = 25 ($C_2H^+$). If the neutral fragments are NH + H, then its absence

Table III-2. Appearance potentials calculated for the primary fragment ions observed by Franklin, et al. in the $CH_3CN$ mass spectrum.

| m/e | Assumed Formula | Assumed Neutral Fragments | Appearance Potential |
|---|---|---|---|
| 12 | $C^+$ | $HCN+H_2$ | 19.02 eV |
| 13 | $CH^+$ | HCN+H | 19.4 eV |
| 14 | $CH_2^+$ | HCN | 14.90 eV |
| 15 | $CH_3^+$ | CN | 14.96 eV |
| 24 | $C_2^+$ | $N+H_2+H$ | 26.8 eV |
| | $C_2^+$ | $NH_2+H$ | 23.6 eV |
| | $C_2^+$ | $NH+H_2$ | 23.1 eV |
| | $C_2^+$ | $NH_3$ | 19.3 eV |
| 25 | $C_2H^+$ | NH+H | 22.0 eV |
| | $C_2H^+$ | $N+H_2$ | 21.22 eV |
| | $C_2H^+$ | $NH_2$ | 18.1 eV |
| 26 | $CN^+$ | $CH_3$ | 19.1 eV |
| 26 | $C_2H_2^+$ | NH | 16.2 eV |
| 27 | $HCN^+$ | $CH_2$ | 18.1 eV |
| 27 | $C_2H_3^+$ | N | 15.6 eV |
| 28 | $H_2CN^+$ | CH | 17.9 eV |
| 38 | $C_2N^+$ | $H_2+H$ | 19.1 eV |
| 39 | $HC_2N^+$ | $H_2$ | 15.1 eV |
| 40 | $H_2C_2N^+$ | H | 14.01 eV |

from the photoionization mass spectrum would be explained by the high calculated appearance potential of 22.0 eV. An appearance potential of 21.22 eV is calculated if the assumed neutral fragments are N + $H_2$. This energy falls right on the HeI resonance line. Since m/e = 25 is a fragment ion, the cross section for its formation should be very small at threshold. As a result, the intensity of the signal might be too weak to be observable when the HeI lamp is used as a source of ionizing radiation. Were the true value closer to the third and lowest calculated appearance potential, the cross section would be large enough at 21.2 eV to make the ion observable. Thus, it is concluded that the $C_2H^+$ (m/e = 25) appearance potential is at least 21.22 eV.

Several fragment ion peaks are really comprised of two different ions. In the electron bombardment mass spectrum of $CH_3CN$, Franklin and coworkers concluded that m/e = 26 is comprised of approximately 60% $CN^+$ and 40% $C_2H_2^+$ by means of a high resolution time-of-flight mass spectrometer. Similarly, the m/e = 27 peak was found to be approximately 85% $HCN^+$ and 15% $C_2H_3^+$. A glance at Table III-2 shows that the appearance potentials of the ions in each of these pairs differ widely. Such a situation might allow the determination of the P.I.E. curve of the ion with the lowest appearance potential up to the threshold for the formation of the second member of the composite mass peak. However, the total intensity of each of these composite mass peaks is so low that the MSU PIMS apparatus is unable to measure the P.I.E.'s or appearance potentials of any of the ions comprising them.

The other multiple ion mass peak in the $CH_3CN$ mass spectrum is m/e = 28. The two possible ions are $N_2^+$ (ionization potential = 15.58 eV) and $H_2CN^+$. That m/e = 28 contains a high $N_2^+$ component is suggested by the low m/e = 28 intensity in the $CH_3CN$ mass spectrum of Franklin and coworkers and the strong m/e = 32 peak in the photoionization mass spectrum. Efforts were made to remove air from the samples, but they were not completely successful. The calculated appearance potential of $H_2CN^+$ is greater than that of $N_2^+$, so its threshold might show up as a weak (at best) step amidst the well-known strong, sharp autoionization structure of the $N_2^+$ P.I.E.

The decision to study acetonitrile-$d_3$ in addition to the protonated compound was based on the hope that deuterium substitution would help distinguish the ions in the $CH_3CN$ multiple ion mass peaks (m/e = 26,27). Unfortunately, the situation in the $CD_3CN$ mass spectrum is even more complicated than its protonated counterpart. Three possible multiple ion mass peaks may be present: m/e = 26, m/e = 28 and m/e = 30. As in $CH_3CN$, the peak at m/e = 28 is comprised of two low intensity ions mixed with $N_2^+$. The peak at m/e = 30 is probably comprised of $D_2CN^+$ and $C_2D_3^+$, both of which have signals that are too weak to measure meaningfully. The peak at m/e = 26 deserves special comment. Although two ions are possible at this mass, $CN^+$ and $C_2D^+$, only the $CN^+$ fragment is likely to be present at the ionizing energy used here as the appearance potential of $C_2D^+$ is close to that of $C_2H^+$. This would explain the very low relative intensity of m/e = 26 ($CN^+$) in $CD_3CN$ in comparison so that of m/e = 26 ($CN^+$ and $C_2H_2^+$) in $CH_3CN$.

Of the remaining primary ions in both photoionization mass spectra, only five in each case were of sufficient intensity to enable meaningful P.I.E. curves to be obtained. The $CH_3^+$ and $CD_3^+$ fragment ions represented the upper sensitivity limit of the MSU PIMS instrument.

The mass spectra of both compounds display peaks that result from reactions between the parent (molecular) ion and the neutral molecule. The pressure and time dependence of these reactions were also studied by Franklin and coworkers. As expected for secondary reactions, they found a squared dependence of the product ion signals on ion source pressure (sample pressure) and the residence time of the ions in the source. These ion-molecule reactions are not of interest to this study. However, the reaction

$$H(D)_3CCN^+ + H(D)_3CCN \rightarrow H(D)_4CCN^+ + H(D)_2CCN \qquad (1)$$

proved to be particularly troublesome. The presence of an ion at m/e = 42 in $CH_3CN$ and m/e = 46 in $CD_3CN$ made it necessary to employ relatively high mass resolution even at ionizing energies below the appearance potential of the first fragment ion. Franklin and coworkers reported that the appearance potential of the $CH_4CN^+$ ion is the same as the first ionization potential of the neutral molecule, which indicated that the reaction is at least thermoneutral if not exoergic. This was confirmed by Haney and Franklin, who estimated the $\Delta H°$ of reaction (1) to be -25 kcal/mol in a later study.[22] A more serious problem caused by reaction (1) is that it diminishes the intensity of the parent ion signals at higher source pressures and longer ion source residence times (lower repeller voltages). This is dramatically demonstrated in Table III-3. Whereas the mass spectra in Table III-1 were measured under conditions of low source pressure and high repeller voltage, the $CD_3CN$ mass spectrum in Table III-3 was measured at a repeller voltage of +0.5 V relative to the ion source potential and a source pressure of 0.8 mtorr. Note that the relative intensities of the m/e = 58, m/e = 46 and m/e = 42 peaks are 4, 36 and 5 times greater than that of the parent ion (m/e = 44), respectively. In addition, a second complication may result. Since the neutral product of reaction (1) is $CH_2CN$, the $CH_2CN^+$ signal may be enhanced by direct ionization of this fragment. Obviously, a good solution to this problem would be to measure the P.I.E.'s of the molecular and fragment ions under the conditions of Table III-1. However, under those conditions the intensity of the parent ion signal at the peak of the Hopfield continuum (815 Å, 15.2 eV) is only 3 x $10^{-11}$ amps or about 100 counts/sec. Since the intensities of many of the fragment ion signals are less than 10% of the parent ion signal, a compromise had to be reached. Consequently, the experimental results presented in the next section were obtained at an intermediate average source pressure of approximately 0.5 mtorr and a potential of +10 V on the repeller with respect to the ion source potential. Under these conditions, the intensity of m/e = 41 (44) relative to the intensity of m/e = 42 (46) is approximately 3:1 at an ionizing energy of 15.2 eV. This minimized the effects of reaction (1) while allowing the achievement of better signal-to-noise ratios in more reasonable (though still long) times.

One might expect that the complete mass spectrum of acetonitrile would display negative ions in addition to the parent ions just discussed, due to the presence of a -CN group with its pseudohalogen characteristics. In their earlier incomplete PIMS study of acetonitrile, Dibeler and Liston searched unsuccessfully for negative ions resulting from ion-pair formation processes.[23] At the time of this writing the MSU PIMS apparatus is not yet

Table III-3. Acetonitrile-$d_3$ mass spectrum at a source pressure of 0.8 mtorr and a repeller voltage of +0.5 V.

| m/e | Intensity Relative to $CD_3CN^+$ (m/e=44) |
|---|---|
| 12 | trace |
| 14 | 0.01 |
| 16 | 0.15 |
| 18 | 0.4 |
| 26 | --- |
| 28 | 0.13 |
| 30 | 0.05 |
| 32 | 0.075 |
| 38 | 0.010 |
| 40 | 0.050 |
| 42 | 5.0 |
| 44 | 1 |
| 46 | 36.3 |
| 54 | 0.035 |
| 56 | 0.25 |
| 58 | 4.13 |

set up for negative ion detection. However, attempts were made to detect the positive fragment from the reaction

$$H(D)_3CCN + h\nu \rightarrow H(D)_3C^+ + CN^-. \qquad (2)$$

The $CH_3^+$ appearance potential in reaction (2) may be calculated in the following way:

$$A.P.(CH_3^+) = D_0(H_3C\text{-}CN) + I.P.(CH_3) - E.A.(CN) \qquad (3)$$

or

$$A.P.(CH_3^+) = 5.26\ eV^{24} + 9.842\ eV^{25} - 3.82\ eV^{26} \qquad (4a)$$

$$A.P.(CH_3^+) = 11.28\ eV \text{ or } 1099\ \text{Å}, \qquad (4b)$$

where $D_0(H_3C\text{-}CN)$ is the bond energy of the acetonitrile carbon-carbon bond, $I.P.(CH_3)$ is the first ionization potential of $CH_3$, and E.A.(CN) is the electron affinity of the cyanogen radical. Searches were made for $CH_3^+$ and $CD_3^+$ in this wavelength region using atomic impurity lines in the Hopfield continuum and the $H_2$ pseudo continuum as sources of radiation. The results, like those of Dibeler and Liston, were negative. However, as the light sources in this wavelength region are comparatively weak, absence of ion-pair formation is by no means conclusively demonstrated.

## B. The Photoionization Efficiency Curves

Acetonitrile was the subject of two early photoionization (PI) studies[27,28] in addition to the PIMS investigation mentioned earlier.[23] Because these two early works lacked mass analysis, they were limited to the determination of the first ionization potential. In their complete PIMS study of acetonitrile, Dibeler and Liston[23] reported only the first ionization potential and the appearance potentials of the three most intense fragment ions - $H_2CCN^+$, $HCCN^+$, and $CH_2^+$. Moreover, they did not present photoionization efficiency curves for any of these ions. Their data were reported in the second part of a paper the primary objective of which was the determination of the heat of formation of the cyanogen radical (CN) by means of a PIMS study of HCN. Their inability to measure the appearance potentials of the $CH_3^+$ and $CN^+$ fragments, which would have provided a second independent measurement of the cyanogen radical's heat of formation, probably caused them to lose interest in further work on acetonitrile. Moreover, the first 70 Å of the parent ion P.I.E. curve lie in a wavelength region where both the He Hopfield continuum and the $H_2$ pseudo-continuum are of low intensity (950 Å - 1020 Å). This makes studies of the $CH_3CN^+$ threshold region very difficult.

The goal of the present investigation was to provide as complete a PIMS study of acetonitrile as possible, considering the nature of the mass spectrum. It is unfortunate that the appearance potential and P.I.E. curve of the $CN^+$ fragment could not be observed. However, it was possible to measure them for the $CH_3^+$ fragment ion, marking the first time that they have been reported. A knowledge of the $CH_3^+$ appearance potential allows the calculation of the carbon-carbon bond energy, $D_0(H_3C\text{-}CN)$, of acetonitrile. This is an important quantity to know when trying to unravel the energetics of the interstellar chemistry of acetonitrile. In addition the work was extended to include the deuterated compound.

Preliminary experiments revealed that the P.I.E. curves of the deuterated ions were within experimental error identical to those of their protonated counterparts. For this reason, only the threshold regions of their P.I.E. curves will be presented here, except for the deuterated molecular ion $CD_3CN^+$, where the complete curve is shown. All appearance potentials were measured with 100 micron entrance and exit slits on the monochromator. This arrangement provided a photon bandwidth of 0.83 Å. In addition, the P.I.E. curves of $CH_3CN^+$, $CD_3CN^+$ and $CH_2CN^+$ from threshold to 600 Å (20.7 eV) were obtained under these resolution conditions. The remaining ions were found to be of low intensity and to possess essentially featureless P.I.E. curves. Consequently, their overall P.I.E. curves were obtained using 300 micron entrance and exit slits (2.5 Å photon bandwidth). When 100 micron slits were in use, measurements were taken every 0.25 Å. In the case of 300 micron slits, data were collected every 0.5 Å. As mentioned in Chapter II-B, the P.I.E. curves have been corrected for light source, sample pressure and detector drift, stray light detector drift and stray light. In addition, the overall P.I.E. curves were corrected for the wavelength dependence of the photon transducer sensitivity by means of the sodium salicylate - photomultiplier detection system. With the exception of $H_2CCN^+$, the threshold regions of all of the fragment ion P.I.E. curves were measured with an electron multiplier as the photon transducer. This was done in order to take advantage of the electron multiplier's lower levels of noise and dark current in these regions of weak ion intensity. The lack of correction for the wavelength dependence of the electron multiplier sensitivity is not critical over the narrow threshold ranges (20 Å to 40 Å) and does not change the positions of the thresholds themselves.

Figures III-1 and III-2 depict the thresholds and first 80 Å of the P.I.E. curves of $CH_3CN^+$ and $CD_3CN^+$, respectively. In addition, the thresholds have been replotted on an expanded vertical scale in order to facilitate measurement of the first ionization potentials. Using the

Figure III-1. Threshold region of the $H_3CCN^+$ P.I.E. curve.

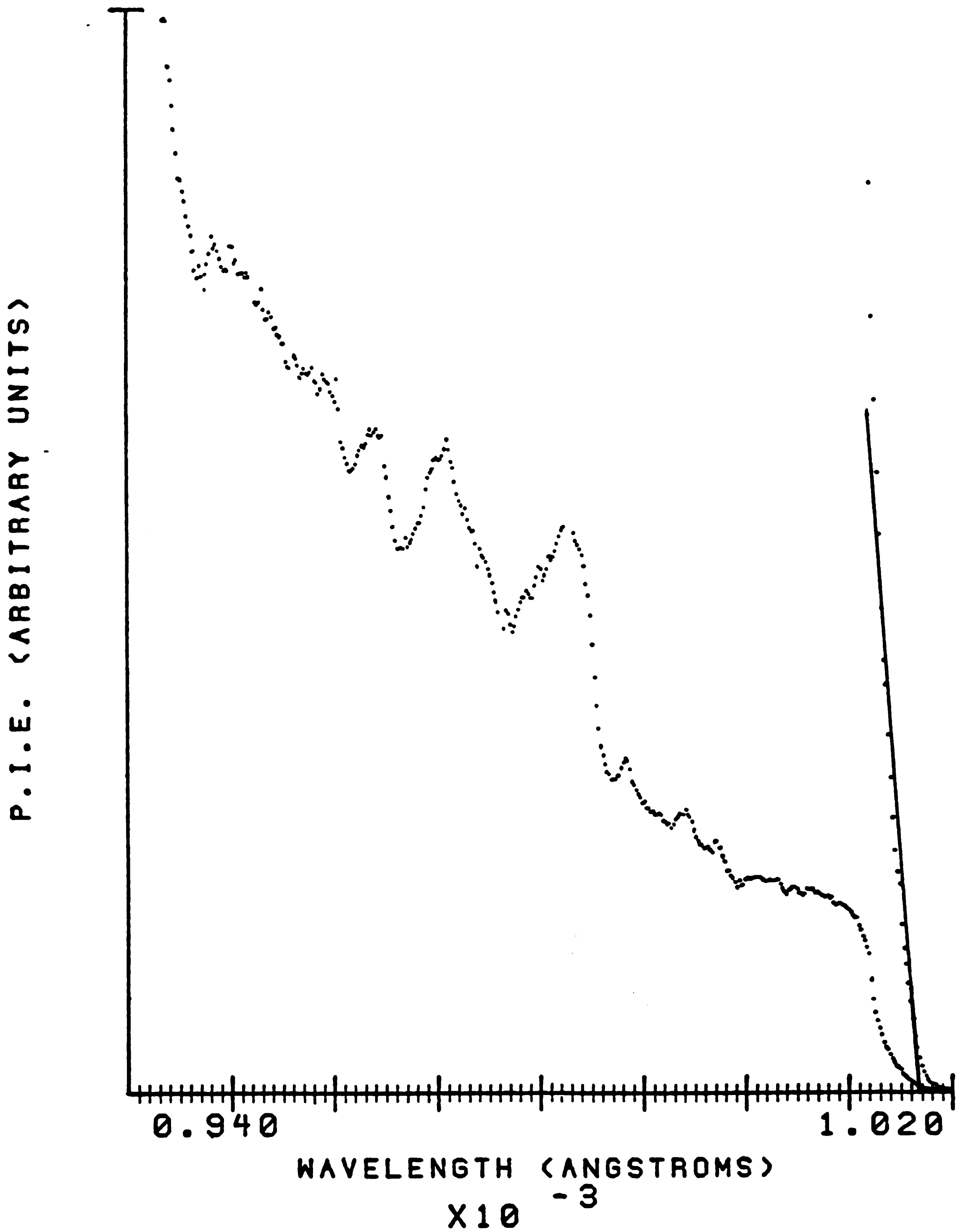

P.I.E. (ARBITRARY UNITS)
0.940
1.020
WAVELENGTH (ANGSTROMS)
X10 -3

Figure III-2. Threshold region of the $D_3CCN^+$ P.I.E. curve.

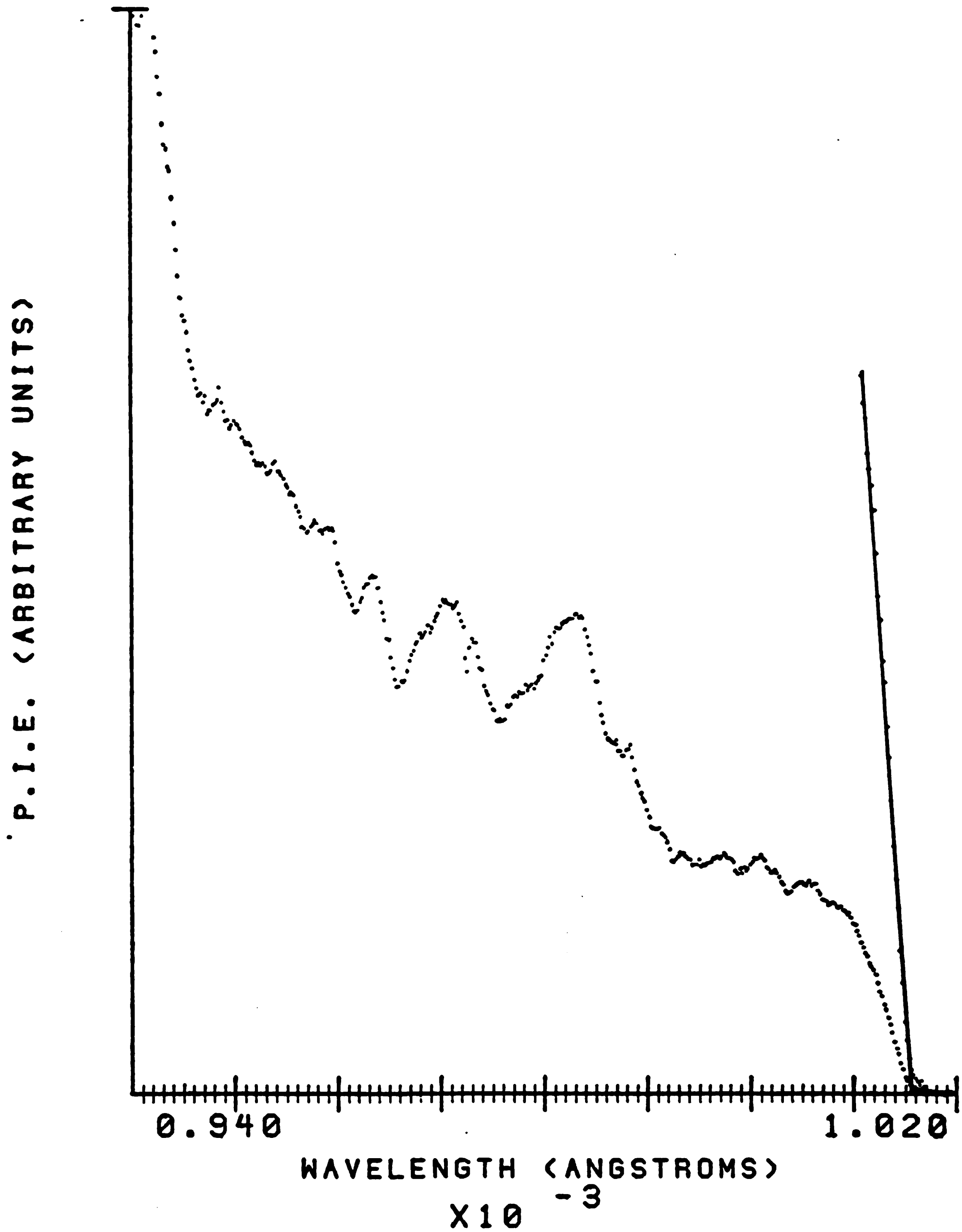
P.I.E. (ARBITRARY UNITS)
0.940
1.020
WAVELENGTH (ANGSTROMS)
X10 $^{-3}$

method of Guyon and Berkowitz[32], we may assume that the 0°K photoionization threshold is a step function and obtain the ionization potentials by extrapolating the linear portion of the P.I.E. curves to the horizontal axis and subtracting 0.4 Å to compensate for the half-width of the photon beam. The values so obtained are compared to the current literature values in Table III-4. The value of the acetonitrile first ionization potential reported here agrees well with previous determinations. A few remarks on some of the other studies are in order. The low resolution photoelectron spectroscopic study of Frost, Herring, McDowell and Stenhouse[30] seems to be too low, especially since the value reported is a vertical ionization potential rather than the adiabatic value reported here. The value reported by Watanabe, Nakayama and Mottl[27] is probably high, because the ion current was measured between two parallel plates across which a low voltage was applied. The sensitivity of such an arrangement is undoubtedly much lower than that of an electron multiplier. Finally, the precision of the value reported by Nicholson[28] is probably unfounded since the width of the photon beam was 4.4 Å in contrast to 0.83 Å in the present case.

The acetonitrile-$d_3$ ionization potential reported by Lake and Thompson in a photoelectron spectroscopic study is the only value currently in the literature.[29] It is probably higher than the present result because it

Table III-4. A comparison of the values for the first ionization potential of $CH_3CN$ and $CD_3CN$ as reported in this and other works.

| Molecule | Reported Value | Method | Reference |
|---|---|---|---|
| $CH_3CN$ | $12.20_2 \pm 0.005$ eV | PIMS | This work |
| | $12.19 \pm 0.01$ eV | PIMS | 23 |
| | $12.205 \pm 0.004$ eV | PI | 28 |
| | $12.22 \pm 0.01$ | PI | 27 |
| | $12.20 \pm 0.01$ | PE | 29 |
| | 12.18 | PE | 30 |
| | 12.21 | PE | 31 |
| $CD_3CN$ | $12.21_4 \pm 0.005$ eV | PIMS | This work |
| | $12.23 \pm 0.01$ eV | PE | 29 |

is a vertical ionization potential. It is interesting that acetonitrile-$d_3$ was also studied in reference 30, but no result was reported. The very small difference in first ionization potentials between the protonated and deuterated compounds is expected. All of the photoelectron (PE) studies have revealed that the most weakly bound electron of acetonitrile is in the CN group $\pi$-orbital (3e).[33,34] Three vibrational modes of the ion are excited upon removal of this electron. They have been assigned to the CN stretching mode ($\nu_2$), the symmetric $CH(D)_3$ deformation mode ($\nu_3$) and the C-C stretching mode ($\nu_4$) with wavenumbers 2010 $cm^{-1}$, 1430 $cm^{-1}$ and 810 $cm^{-1}$ in $H_3CCN^+$, respectively.[31] The same modes in the neutral are 2267 $cm^{-1}$, 1385 $cm^{-1}$ and 920 $cm^{-1}$, respectively.[35] The mode that appears in the PE spectrum with the most intensity is $\nu_2$. In comparison, $\nu_3$ is only very weakly excited. These results suggest that the $\pi$-orbital is C-N and C-C bonding and weakly C-H antibonding. Thus, the substitution of deuterium for hydrogen should have little effect upon the first ionization potential. The difference is probably due to the small differences in the zero-point energies of the neutrals and ions.

The region immediately above threshold (about 1017 Å) to approximately 990 Å (Figures III-1,2) is difficult to interpret. The small peaks correspond to lines in the $H_2$ pseudo-continuum. They appear because the intensity of the scattered light is nearly equal to the intensity of the incident beam. Apparently, the computer program currently used for data treatment is unable to make the proper corrections in regions of such low light intensity. The overall shape of the P.I.E. curves in this region is suggestive of a vibronic threshold; however the onset is not clear. This is probably due to the fact that three vibrational modes are excited in this region (see the previous paragraph). If the $CH_3CN^+$ P.I.E. curve were simply an integral photoelectron spectrum, vibronic thresholds would appear at 1006 Å ($\nu_4$), 1000 Å ($\nu_3$), 995 Å ($\nu_2$) and 993 Å ($2\nu_3$). Weak autoionization structure superimposed on the P.I.E. curves may be masking these thresholds.

The three peaks in the region from 983 Å to 964 Å, with a fourth suggested at 959 Å, undoubtedly are part of a previously unobserved autoionizing Rydberg series that converges to an excited state of the ion. Their positions and the analysis proposed here are presented in Table III-5. Attempts were made to assign this series as converging to one of the vibrationally excited states of the ground state ion ($\tilde{X}^2E$).[33,34] However, the quantum defects calculated from the position of each peak were all completely different (and sometimes absurd as well!). The peaks are not vibronic components of a single member of an autoionizing Rydberg series, because their separation diminishes with increasing energy. Furthermore, the positions of these peaks are unaltered upon deuteration with the exception of the third

Table III-5. Analysis of the autoionizing Rydberg series in $CH_3CN$ and $CD_3CN$.

| Molecule | Assumed Limit | Peak Position (observed) | Quantum Defect (δ) | n |
|---|---|---|---|---|
| $CH_3CN$ | 13.14 eV[29] | 983.0 Å;101,729 $cm^{-1}$ | 0.92 | 6 |
| | 105,981 $cm^{-1}$ | 971.0 Å;102,987 $cm^{-1}$ | 0.95 | 7 |
| | | 964.0 Å;103,734 $cm^{-1}$ | 1.01 | 8 |
| | | 959.0 Å;104,275 $cm^{-1}$ | 0.98 | 9 |
| | Mean δ=0.97 | | | |
| $CD_3CN$ | 13.14 eV | 983.0 Å;101,729 $cm^{-1}$ | 0.92 | 6 |
| | 105,981 $cm^{-1}$ | 971.0 Å;102,987 $cm^{-1}$ | 0.95 | 7 |
| | | 963.5 Å;103,788 $cm^{-1}$ | 0.93 | 8 |
| | | 959.0 Å;104,275 $cm^{-1}$ | 0.98 | 9 |
| | Mean δ=0.95 | | | |

component. In $H_3CCN^+$, this peak lies between vibronic thresholds at 968 Å ($4\nu_3$) and 962 Å ($4\nu_2$), whereas the $4\nu_2$ threshold ($CD_3$ symmetric deformation) lies at a much longer wavelength in the deuterated compound. Perhaps the position of this component of the $H_3CCN$ Rydberg series is slightly distorted by the structure underlying it. The only reasonable choice for the series limit seems to be the threshold for the first electronic excited state of the molecular ion ($\tilde{A}\,^2A_1$).[33,34] PE studies have placed the origin of this excited state at 13.14 eV (943.6 Å) for both the protonated and deuterated ions.[29] This corresponds to approximately the midpoint of the sharp step observed above the Rydberg series. The PE results and CNDO calculations by Frost, et al. suggest that the electron ionized is from the nitrogen "lone-pair" orbital.[30] Although the intensities of the peaks decrease with energy, they are on a "baseline" that is increasing with energy. This is probably the result of the series being superimposed over several vibronic thresholds of the ionic ground state. These thresholds have all been identified in the PE spectra (best seen in Reference 31). In addition to the autoionization structure, the broad structureless region in the P.I.E. curve between 959 Å and 943 Å probably results from further vibronic thresholds, masked by higher unresolvable members of the autoionizing Rydberg series. These observations, plus the magnitudes of the calculated quantum defects, lead to the assignment of these peaks to part of an ns$\sigma$ autoionizing Rydberg series, where n = 6-9. That is, the series is formed by the excitation of an electron from the nitrogen "lone-pair" orbital of the neutral molecule into an empty s-orbital with subsequent autoionization.

It is difficult to test the validity of this assignment since the vacuum ultraviolet spectroscopic data on acetonitrile are poor and far from complete. The most recent vacuum UV absorption study is thirty-one years old and terminates at 1060 Å.[36] Three Rydberg peaks were observed and assigned an incorrect convergence limit of 11.96 eV. No hint of lower members of the series identified in this work was observed. Recently, an electron impact energy loss spectrum of acetonitrile was reported.[37] The energy resolution was only 100 meV, but three Rydberg series converging to the ground state of the molecular ion were observed. Calculation of the energies of the n = 3, 4 and 5 components of the series identified here, suggests that the electron impact spectrum should display peaks at 9.93 eV, 11.69 eV and 12.31 eV, respectively. There are peaks in all three of these regions, but the energy resolution is insufficient to distinguish these features from the other series suggested by the authors as contributors to the broad bands which are observed.[37] The most interesting aspect of the electron impact spectrum is a broad, weak "band" that cuts-off at 13.14 eV, the threshold of the $\tilde{A}\,^2A_1$

state of the parent ion. The lower energy limit of the band is 12.55 eV. It thus encompasses the region of the series observed in this work. The resolution of the electron impact study was too low to resolve this feature, but it is interesting to note that a shoulder and peak on it correspond roughly in energy to the n = 6 and 7 members of the proposed ns$\sigma$ series.

The only disquieting aspect of the assignment proposed here is that the n = 5 component, which should fall within the range of the P.I.E. curve at 1006 Å, is not observed. Provided that the proposed assignment is correct, a possible explanation is that the n = 5 component has been completely depopulated by predissociation into neutral fragments. The broadness and low intensity of the observed peaks suggest that the entire series (within the limits of the P.I.E. curve) is subject to rapid predissociation. Indeed, if this were not the case, the threshold of the $\tilde{A}^2A_1$ state would be unobservable, because the series would converge smoothly to the $\tilde{A}^2A_1$ limit without displaying a discontinuity at that point.[5a] It seems reasonable to suggest that the n = 5 member of the series is crossed by a repulsive potential surface of the neutral molecule. In such a case, it would be completely depopulated while the higher energy members of the series would be predissociated to a lesser extent due to their greater separation from the repulsive surface.

The $H_3CCN^+$ and $D_3CCN^+$ P.I.E. curves from threshold to 600 Å are plotted in Figures III-3 and III-4, respectively. As with the threshold regions, they are completely identical. Other than the steep step at 943.6 Å (13.14 eV), no additional thresholds are observed. It is worth noting that from 600 Å to 945 Å the P.I.E.'s are remarkably similar to the $HCN^+$ P.I.E. curve reported by Dibeler and Liston along with their acetonitrile data.[23] The overall decrease in the P.I.E.'s at shorter wavelengths is probably due to the formation of fragment ions. Indeed, all of the higher energy bands (above the 13.14 eV band) in the PE spectrum are highly predissociated. Very weak autoionization structure is present in the region from 820 Å to 850 Å. This structure may represent one or more Rydberg series whose limit is the second electronic excited state ($\tilde{B}\,^2E$)[33,34] of the parent ion. All of the PE spectroscopic studies have placed this threshold at 15.13 eV or 819.5 Å. The weakness of this structure is another indication of the dominance of predissociation in this energy region.

## $H_2CCN^+$ and $D_2CCN^+$

The threshold regions of the $H_2CCN^+$ and $D_2CCN^+$ P.I.E. curves are pictured in Figures III-5. and III-6, respectively. In common with most fragment ion P.I.E.'s, they are approximately linear sloping curves with thermal tailing at threshold. Guyon and Berkowitz[32] have shown that

Figure III-3. The $H_3CCN^+$ P.I.E. curve from threshold to 600 Å.

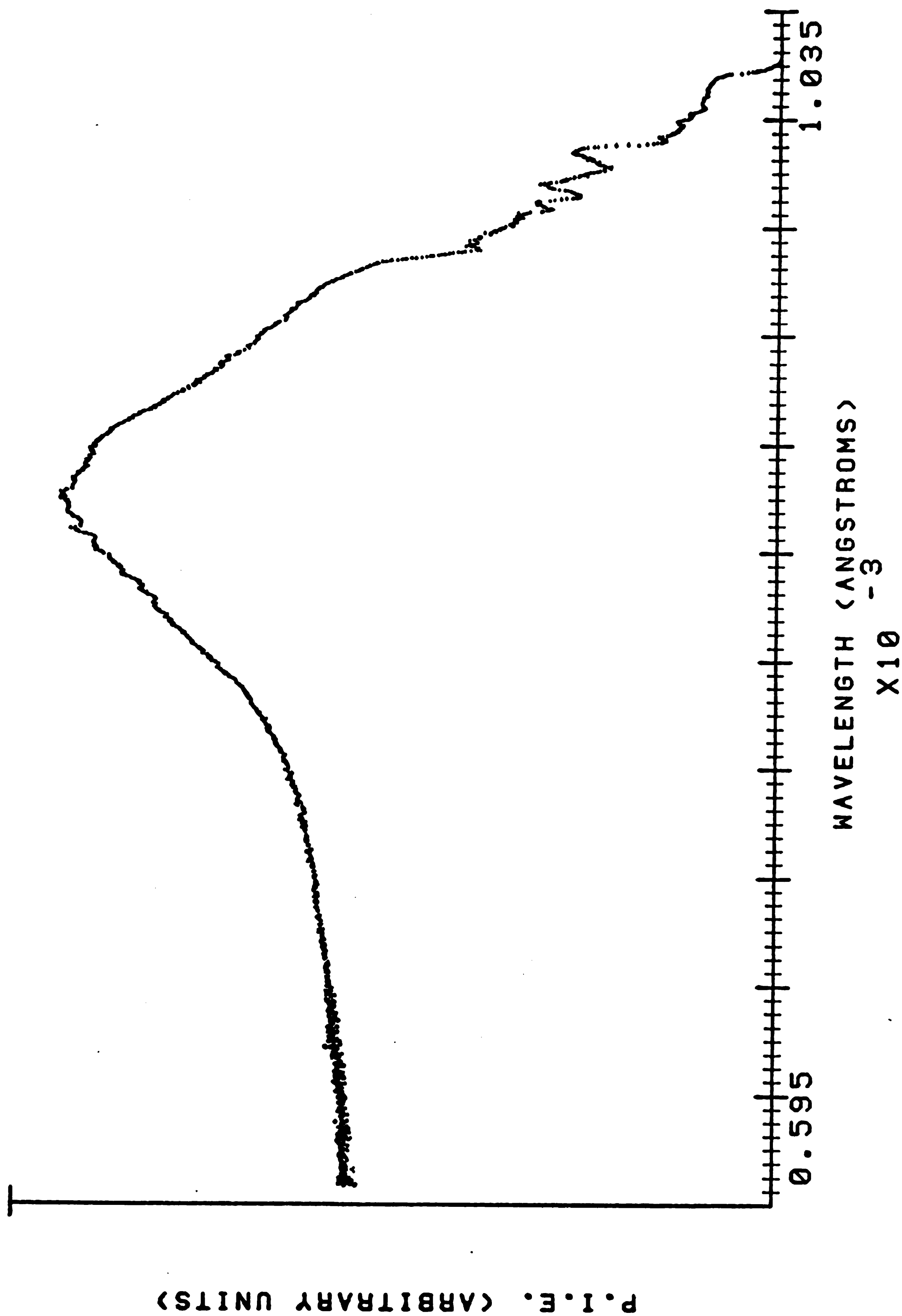

0.595
1.035
WAVELENGTH (ANGSTROMS)
X10 -3
P.I.E. (ARBITRARY UNITS)

Figure III-4. The $D_3CCN^+$ P.I.E. curve from threshold to 600 Å.

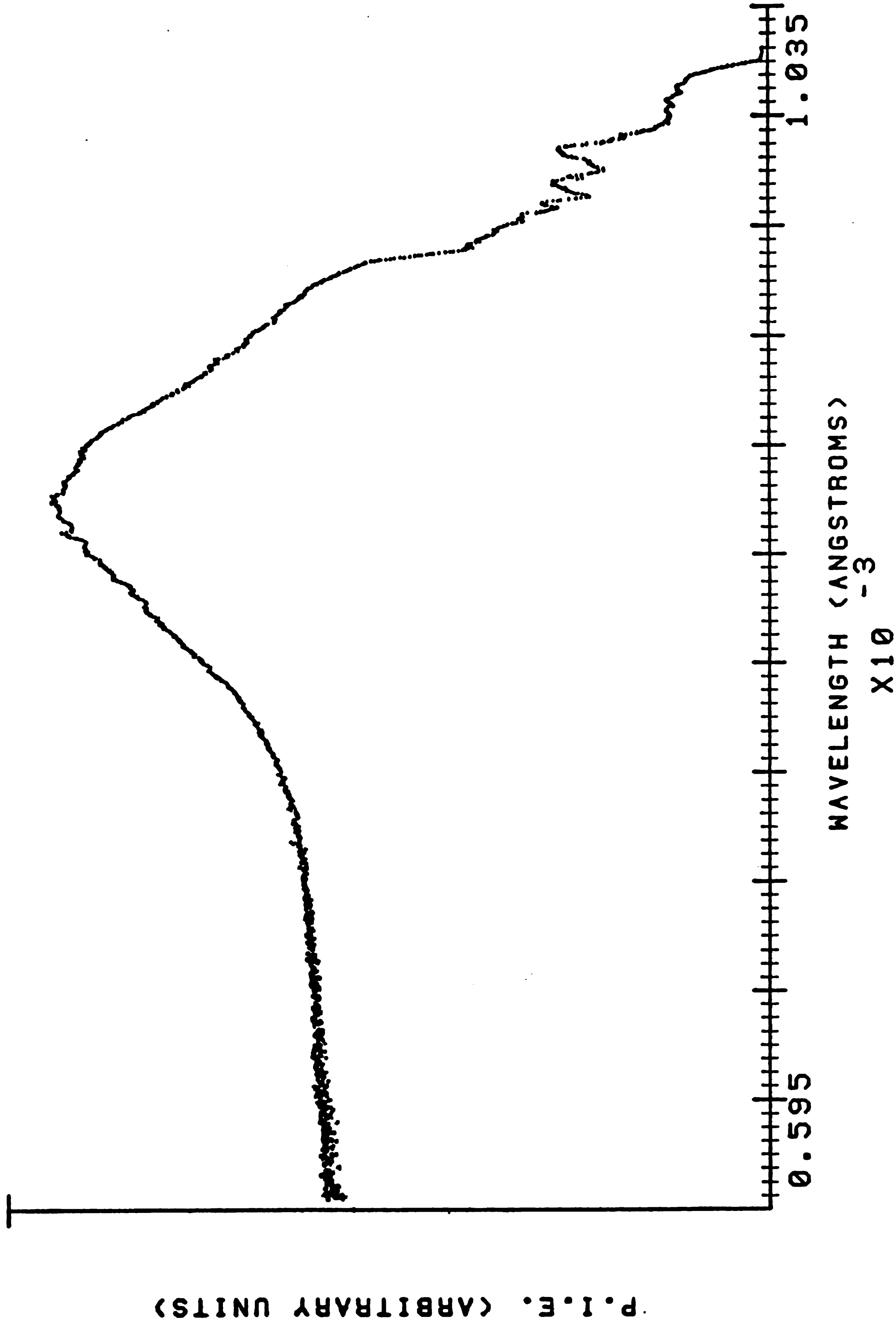
P.I.E. (ARBITRARY UNITS)
WAVELENGTH (ANGSTROMS)
X10 -3
0.595
1.035

Figure III-5. Threshold region of the $H_2CCN^+$ P.I.E. curve.

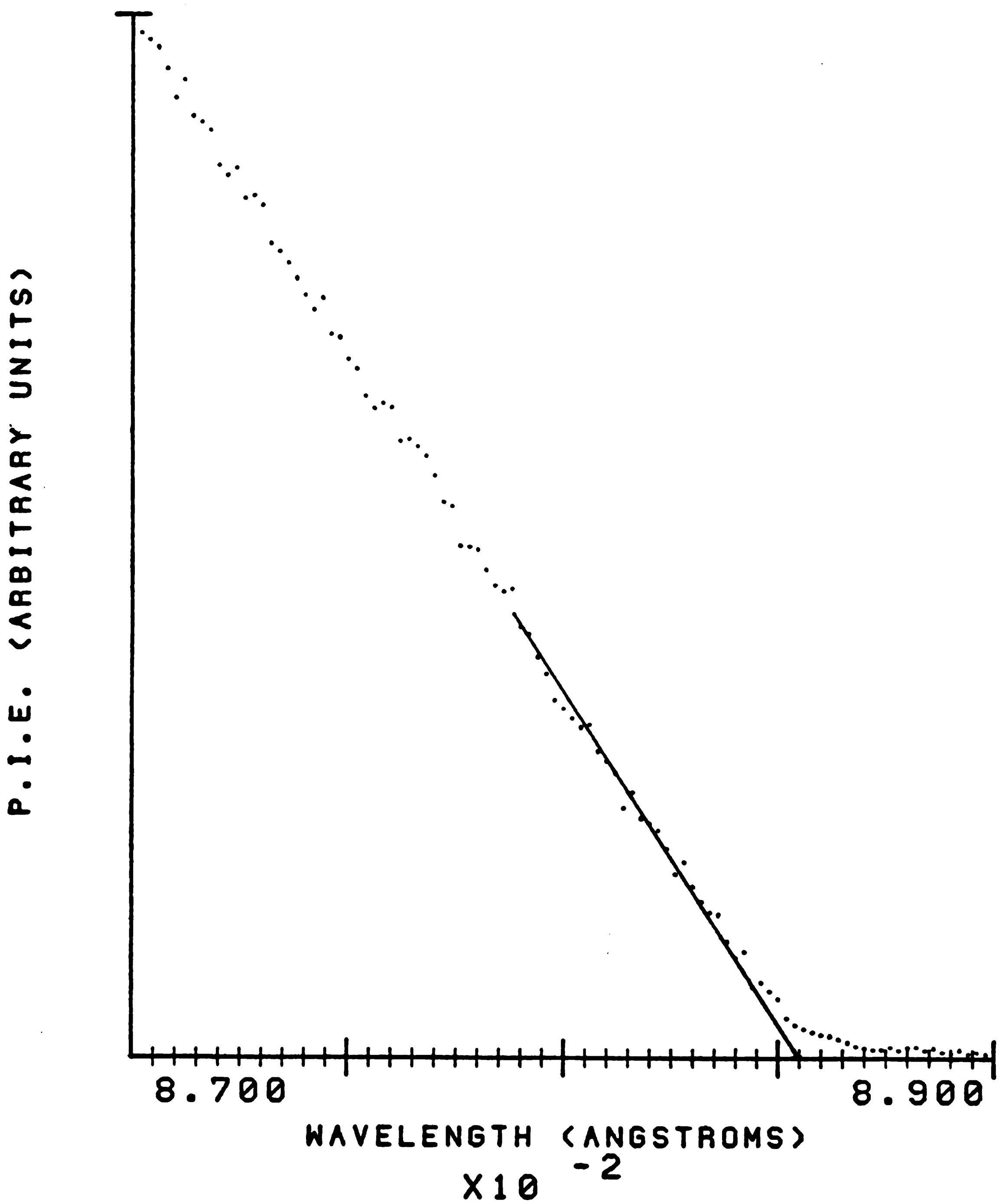
P.I.E. (ARBITRARY UNITS)
8.700
8.900
WAVELENGTH (ANGSTROMS)
X10 -2

Figure III-6. Threshold region of the $D_2CCN^+$ P.I.E. curve.

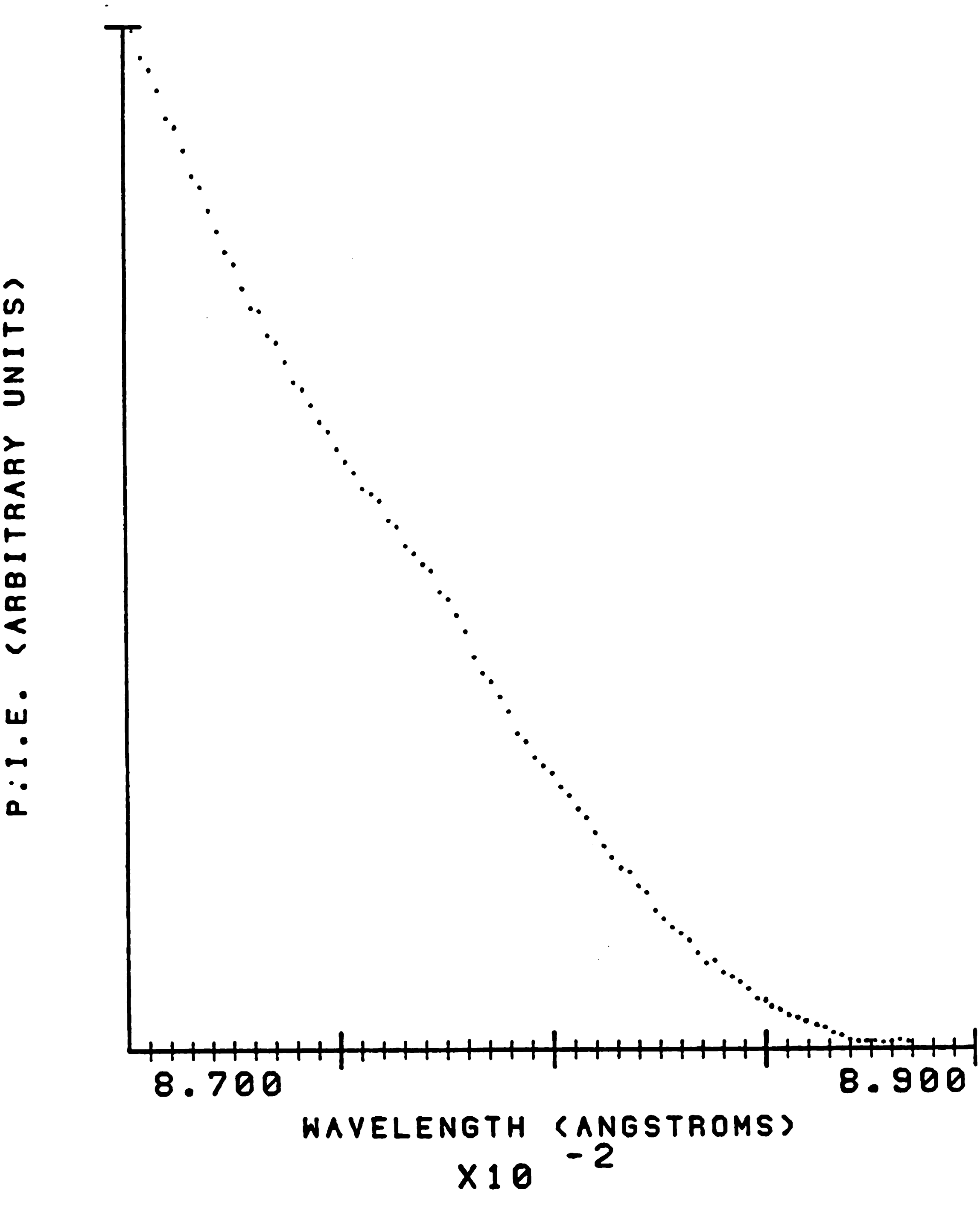
P.I.E. (ARBITRARY UNITS)
8.700
8.900
WAVELENGTH (ANGSTROMS)
X10 -2

the thermal tail is caused by the photoionization of molecules whose rotational energy is greater than the average rotational energy at the temperature of the experiment (3/2 kT). Since the number of molecules in a given rotational state decreases rapidly as their energy above 3/2 kT increases, the observed length of the thermal tail is dependent upon the sensitivity of the apparatus used. It was also shown that the actual appearance potential at the temperature of the experiment may be found by extrapolating the linear portion of the P.I.E. curve to the horizontal axis. If all three rotational degrees of freedom are able to provide energy for the fragmentation of the parent ion, the appearance potential determined by extrapolation will be 3/2 kT lower than the 0°K appearance potential. Of course, it is not always valid to assume that all three of an ion's degrees of rotational freedom are able to participate in a given fragmentation process. One way to determine how many degrees of rotational freedom are taking part in a given fragmentation is to measure the appearance potential at several temperatures.[46] The differences between appearance potentials measured at different temperatures will correspond approximately to n/2 k$\Delta$T, where n is the number of rotational degrees of freedom participating in the fragmentation. An overview of the literature would show that the majority of ionic fragmentations take place with the participation of all rotational degrees of freedom.

For this reason, the acetonitrile appearance potentials presented here will be corrected for 3/2 kT since it is only possible to perform experiments at the ambient temperature with the present ion source. Strictly speaking, the half-width of the photon beam should also be subtracted from the wavelength of the appearance potential. However, this amounts to no more than 6 meV when 100 micron slits (0.4 Å half-width) are used at 885 Å, the relevant region in this case. Consequently, this correction is seldom made as it is usually less than the uncertainty of the appearance potential measurement. Of course, this procedure relies on the assumption that the fragments are formed with essentially zero kinetic energy at threshold. Otherwise, the appearance potential obtained is only an upper bound to the thermodynamic value.

By the above extrapolation method, the uncorrected $H_2CCN^+$ appearance potential is 885.5±0.4 Å or 14.002±0.006 eV. When corrected for the average rotational energy at 300 °K (0.039 eV) and the photon beam half-width (0.006 eV) the value of the 0 °K appearance potential is 14.047± 0.006 eV. This compares well to the value of 14.01±0.02 eV reported by Dibeler and Liston.[23] The difference, which is larger than the combined experimental error, can be explained by the presumption that Dibeler and Liston chose the foot of the thermal tail as their uncorrected appearance potential. Indeed, before the publication of Guyon and Berkowitz,[32] this appears to have been the standard procedure of Dibeler's group.[38]

When the appearance potential determined here is combined with the 0 °K heats of formation of $CH_3CN$ (0.979 eV)[39] and H (2.239 eV)[39], a value of 12.787 eV (294.88 kcal/mol) is obtained for the 0 °K heat of formation of $H_2CCN^+$. With Pottie and Lossing's value for the ionization potential of $H_2CCN$, 10.87±0.1 eV[40], 1.92±0.1 eV (44.4 2 kcal/mol) is calculated for the 0 °K heat of formation of $H_2CCN$. In addition, the carbon-hydrogen bond dissociation energy, $D_0(H\text{-}CH_2CN)$, is found to be 3.18±0.1 eV (73.5±1 kcal/mol). All of these values are slightly higher than those calculated by Dibeler and Liston[23] due to the larger appearance potential reported here. The 0 °K appearance potentials of the fragment ions and the derived thermodynamic quantities are summarized in Tables III-6 and III-7 at the end of this chapter, respectively.

The position of the $D_2CCN^+$ appearance potential is less certain, because its P.I.E. curve is less linear than that of $H_2CCN^+$ in the threshold region. The possible values range from 885 Å to 886 Å. If it is assumed that the thermal tails of the $H_2CCN^+$ and $D_2CCN^+$ P.I.E. curves are of equal width, then 886 Å is preferred. The uncorrected appearance potential is estimated to be 885.5±0.5 Å (14.00±0.01 eV), identical to that of $H_2CCN^+$ within experimental error. The corrected 0 °K value is then 14.05±0.01 eV. Unfortunately, the thermodynamic data required to calculate the 0 °K heats of formation of $D_2CCN^+$ and $D_2CCN$ and $D_0(D\text{-}CD_2CN)$ are unavailable. It is reasonable to expect that they will be very close to the corresponding values of their protonated counterparts.

The $H_2CCN^+$ P.I.E. curve from 900 Å to 600 Å is plotted in Figure III-7. Above the threshold region the curve rises sharply. The weak structure between 850 Å and 820 Å (14.6 eV to 15.1 eV) appears to be the same autoionization structure noted in that region of the $H_3CCN^+$ P.I.E. curve. This structure is relatively more intense than the corresponding structure on the parent ion curve, which indicates that these Rydberg levels are autoionizing and rapidly predissociating to form the $H_2CCN^+$ fragment ion. The threshold for the second electronic excited state of the parent ion ($\tilde{B}^2E$) can be observed in the $H_2CCN^+$ P.I.E. curve as the poorly defined step at approximately 820 Å (indicated by an arrow in Figure III-7). The $CH_3CN$ PE spectrum reveals that this and higher electronic states of $H_3CCN^+$ are extensively broadened by predissociation.[31] The abrupt increase in the $H_2CCN^+$ P.I.E. curve at the threshold of the $\tilde{B}^2E$ state of the parent ion is an indication that predissociation of this state contributes to the $H_2CCN^+$ intensity.

After rising until approximately 775 Å, the $H_2CCN^+$ P.I.E. curve tapers off. Presumably, the decrease in intensity results from the formation of fragment ions with

Figure III-7. The $H_2CCN^+$ P.I.E. curve from threshold to 600 Å.

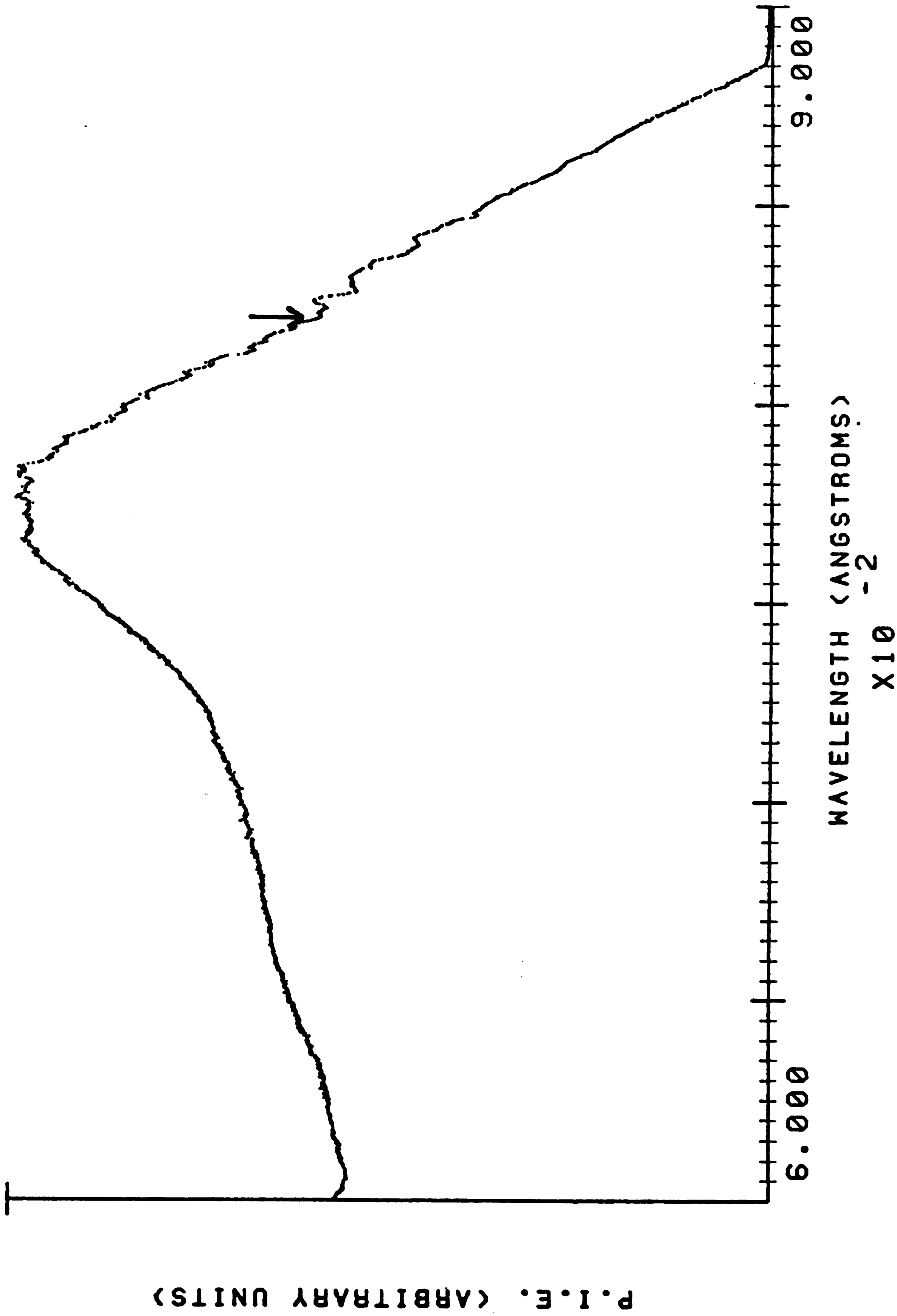
9.000
6.000
WAVELENGTH (ANGSTROMS)
X10 -2
P.I.E. (ARBITRARY UNITS)

higher appearance potentials, but this is not clearly indicated.

The remainder of the fragment ions studied here all have appearance potentials at or just slightly below the threshold of the $\tilde{B}^2E$ state of $H_3CCN^+$ (15.14 eV, 820 Å). In such a situation the thresholds of the P.I.E. curves will normally exhibit kinetic and competition effects. The ion with the largest rate constant for its formation will have the lowest appearance potential. Moreover, the ions may not be detectable until well above their thermodynamic thresholds, because the rate constants for their formation could be too small at that energy to produce an observable number of fragment ions. Such behavior is indicated by a slowly-rising P.I.E. curve with an indeterminant threshold. As demonstrated in the next several sections, the $HCCN^+$, $CH_2^+$ and $CH_3^+$ P.I.E. curves all exhibit this behavior. Furthermore, Haney and Franklin[41] have shown that the $CH_2^+$ fragment is formed with 0.12 eV of kinetic energy upon the dissociative ionization of acetonitrile. It follows that there may be a substantial activation energy for that process. Appearance potentials measured for $HCCN^+$, $CH_2^+$ or $CH_3^+$ may be upper bounds to the adiabatic thermodynamic values.

HCCN$^+$ and DCCN$^+$

The most intense of the three fragment ions whose appearance potentials are near the threshold of the $\tilde{B}^2E$ state of the parent ion is HCCN$^+$(DCCN$^+$). The threshold regions of the HCCN$^+$ and DCCN$^+$ P.I.E. curves are presented in Figures III-8. and III-9, respectively. The structure on both curves is due to atomic lines and irregularities in the Hopfield continuum that have not been successfully corrected for. Both threshold P.I.E. curves are convex, suggesting the kinetic and competition effects discussed earlier. Because the pre-threshold regions are not linear, it is difficult to extrapolate the curves in order to determine the 300 °K appearance potentials. There is an approximately linear portion in the HCCN$^+$ P.I.E. curve between 810 Å and 820 Å. When the P.I.E. curve is extrapolated from this section the uncorrected appearance potential is 821.0±0.5 Å or 15.10±0.01 eV, the relatively large error limits reflecting the uncertainty of the extrapolation. After correction for the temperature shift (3/2 kT) and the photon beam half-width (0.4 Å), the 0 °K appearance potential is 818.5±0.5 Å or 15.15±0.01 eV. The fact that the value is 0.05 eV larger than the one reported by Dibeler and Liston (15.1±0.1 eV)[23] supports the earlier assumption that the differences between the appearance potentials reported here and those of the earlier work are due to the procedures by which the positions of the thresholds were

Figure III-8. Threshold region of the $HCCN^+$ P.I.E. curve.

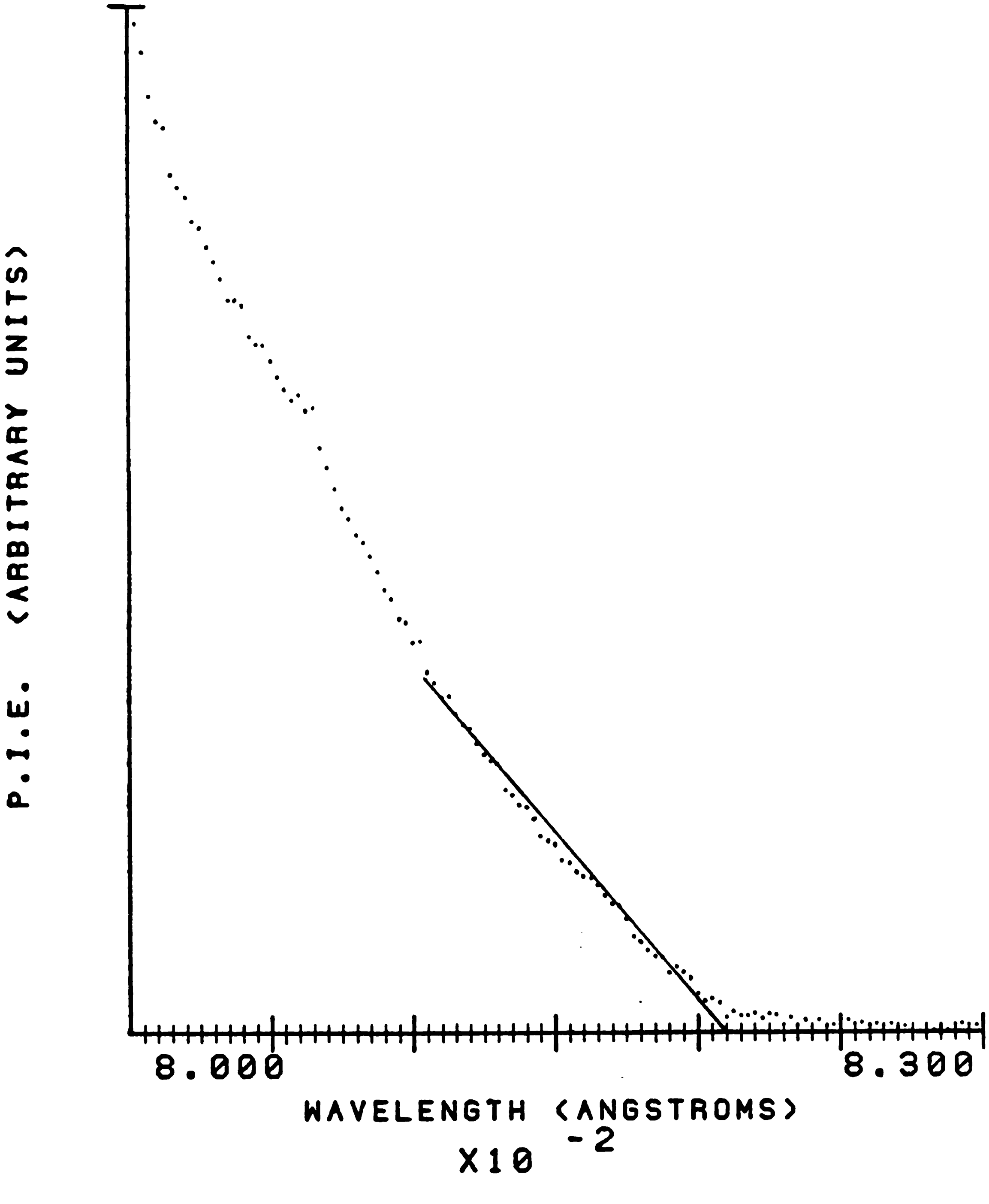
P.I.E. (ARBITRARY UNITS)
8.000
8.300
WAVELENGTH (ANGSTROMS)
X10 -2

Figure III-9. Threshold region of the $DCCN^+$ P.I.E. curve.

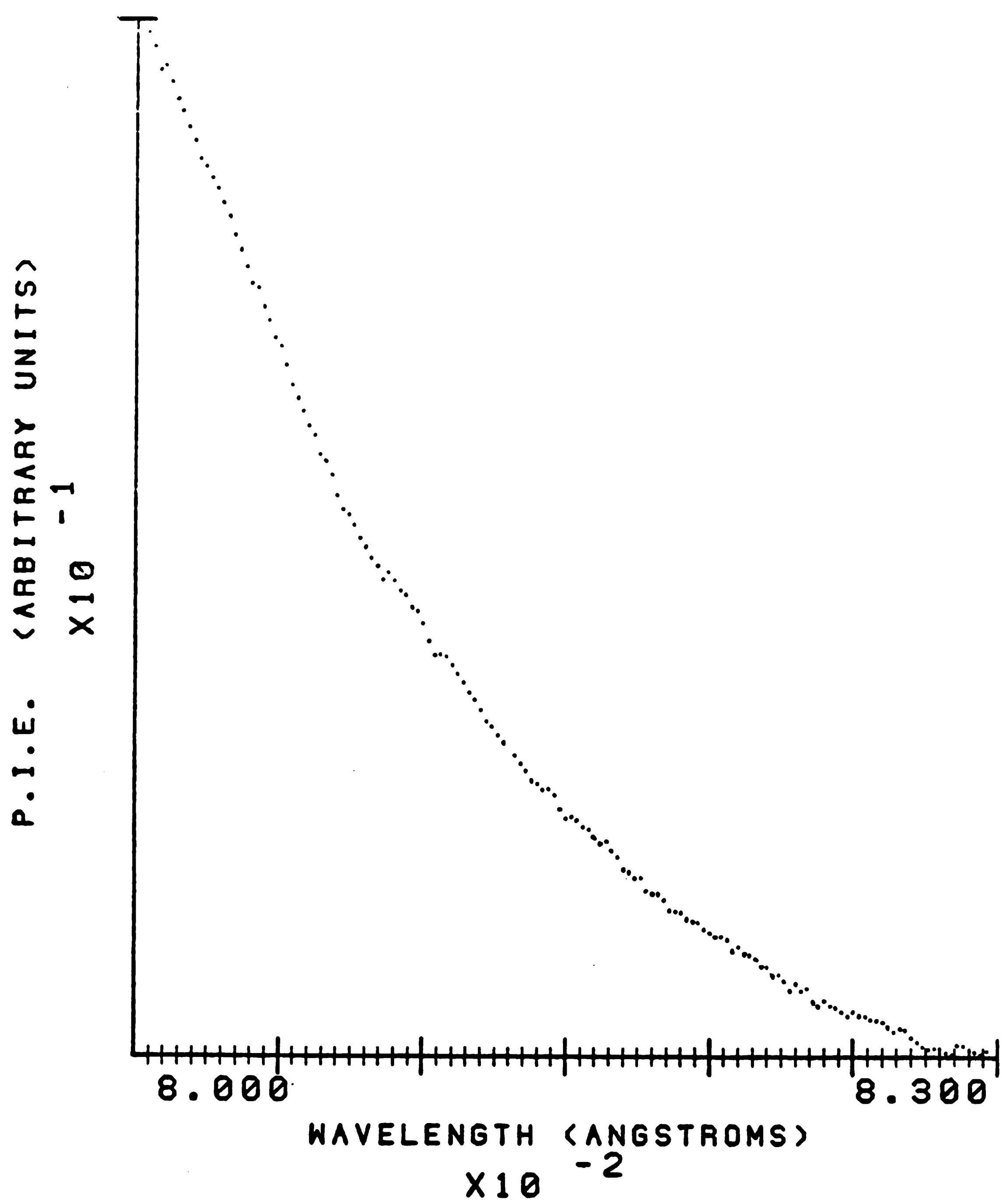
P.I.E. (ARBITRARY UNITS)
X10 -1
8.000
8.300
WAVELENGTH (ANGSTROMS)
X10 -2

estimated. Combining the 0 °K appearance potential with the 0 °K heat of formation of $H_3CCN$ (0.979 eV)[39] gives 16.13±0.01 eV (372.0±0.2 kcal/mol) as the 0 °K heat of formation of $HCCN^+$. Unfortunately, it is impossible to calculate additional thermodynamic quantities, because thermodynamic data on HCCN and $HCCN^+$ are almost non-existent.

The curvature of the $DCCN^+$ P.I.E. curve (Figure III-9) in the threshold region is even more pronounced than that of $HCCN^+$. Since one would expect deuteration to have little effect on the shape of a P.I.E. curve, the increased curvature may be a result of instrumental and sample pressure drift during the experiment. Two extrapolations are possible. If the "linear" portion of the curve between 810 Å and 815 Å is extrapolated to the horizontal axis, the estimated appearance potential is 821.0 Å. If the second linear portion between 818 Å and 823 Å is used, the resulting appearance potential is 826 Å. Both values seem reasonable. The lower wavelength estimate is equal to the uncorrected appearance potential - which is what one might expect from the previous results with the parent ions and $H_2CCN^+$ and $D_2CCN^+$. On the other hand, the difference between 826 Å and the uncorrected appearance potential of $HCCN^+$ (821.0 Å) is not so great as to be unreasonable.[42] Thus, it seems best to report the average value here, 823.5±2.5 Å or 15.06± 0.05 eV. Such error limits make it unnecessary to correct for the photon beam half-width. After correction for

3/2 kT (0.039 eV), the 0 °K $DCCN^+$ appearance potential is 15.10±0.05 eV. The absence of thermodynamic data on DCCN and $DCCN^+$ in the literature renders a test of this value or the derivation of additional thermodynamic parameters impossible.

The $HCCN^+$ P.I.E. curve from threshold to 600 Å is depicted in Figure III-10. The shallow slope in the threshold region is indicative of the presence of kinetic and competition effects. This observation suggests that the $HCCN^+$ and $DCCN^+$ appearance potentials reported here are in reality upper bounds to the true thermodynamic thresholds. The slope of the P.I.E. curve increases at approximately 820 Å (15.12 eV) which is near the threshold of the $\overline{B}\,^2E$ state of the parent ion. Apparently the extensive predissociation of this state, noted in the PE spectrum[31], contributes strongly to the formation of $HCCN^+$. The remainder of the P.I.E. curve is featureless. The scatter at short wavelengths is due to the very weak signal (less than 5 counts/sec). The weak structure around 680 Å is the result of incompletely corrected lines in the Hopfield continuum.

<u>$CH_2^+$ and $CD_2^+$</u>

The threshold regions of the P.I.E. curves of $CH_2^+$ and $CD_2^+$ are shown in Figures III-11 and III-12, respectively. As expected, both curves have long low-energy tails and indefinite thresholds, owing to kinetic and competition

Figure III-10. The $HCCN^+$ P.I.E. curve from threshold to 600 Å.

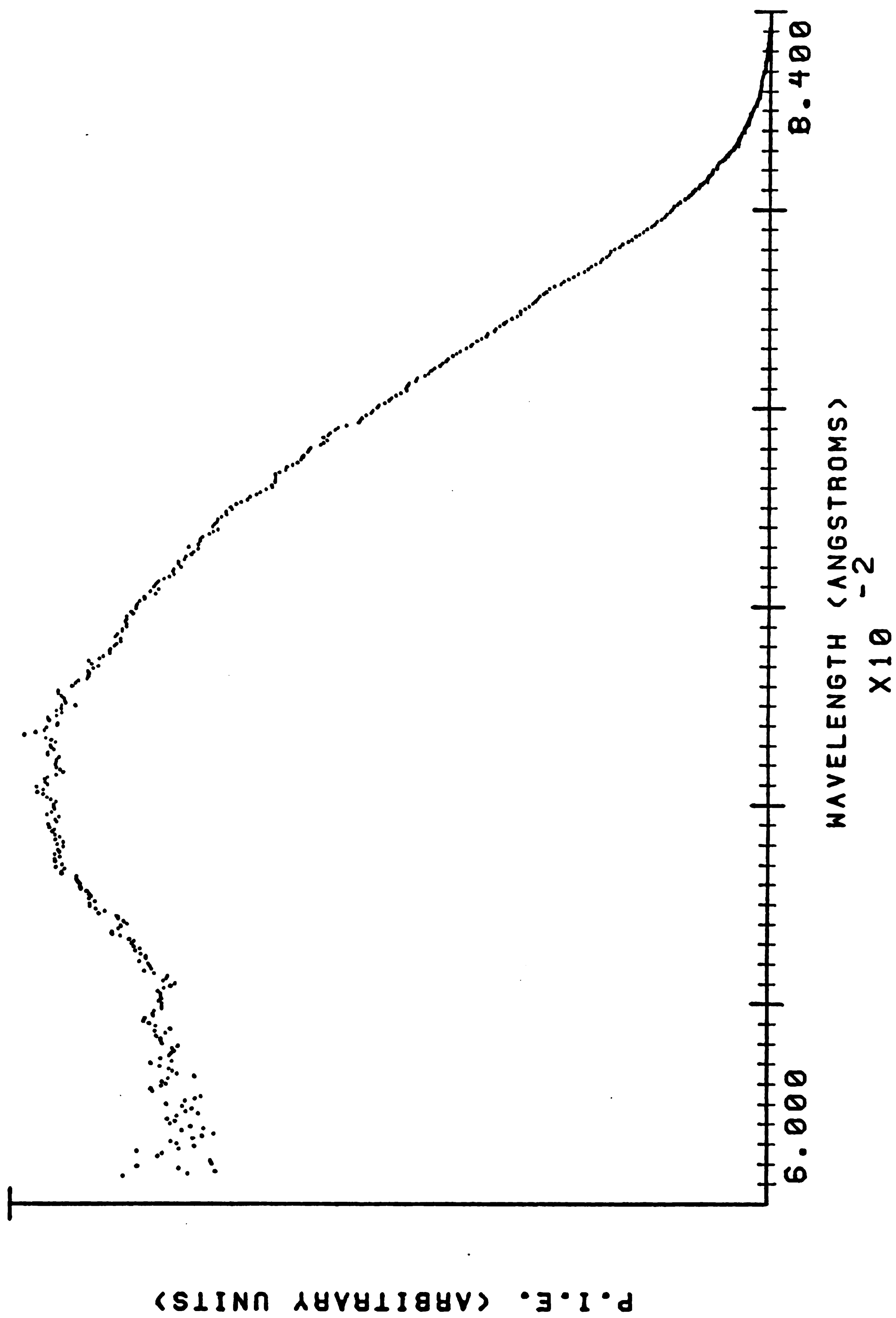
6.000
8.400
WAVELENGTH (ANGSTROMS)
X10 -2
P.I.E. (ARBITRARY UNITS)

Figure III-11. Threshold region of the $CH_2^+$ P.I.E. curve.

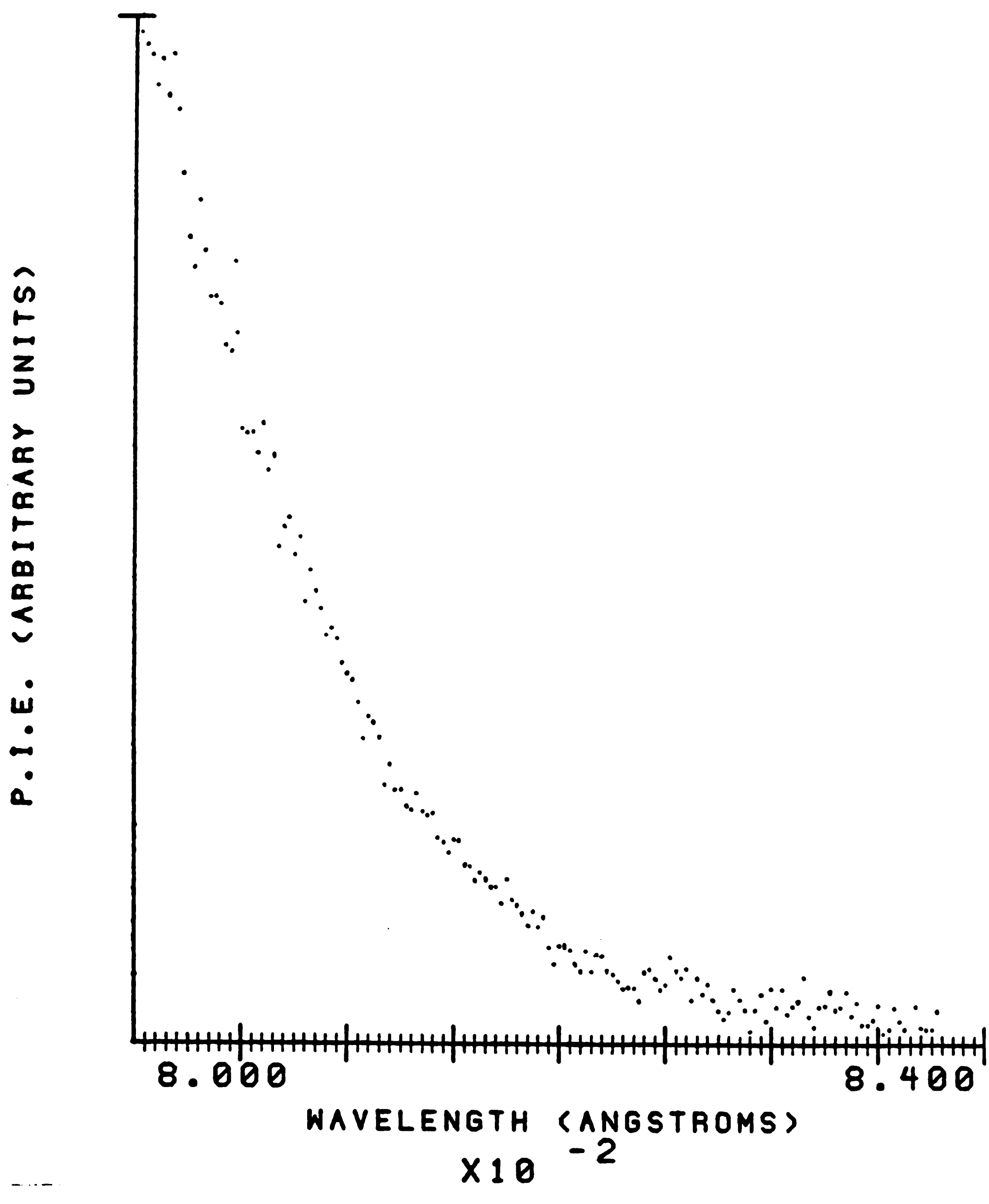
P.I.E. (ARBITRARY UNITS)
8.000
8.400
WAVELENGTH (ANGSTROMS)
X10 -2

Figure III-12. Threshold region of the $CD_2^+$ P.I.E. curve.

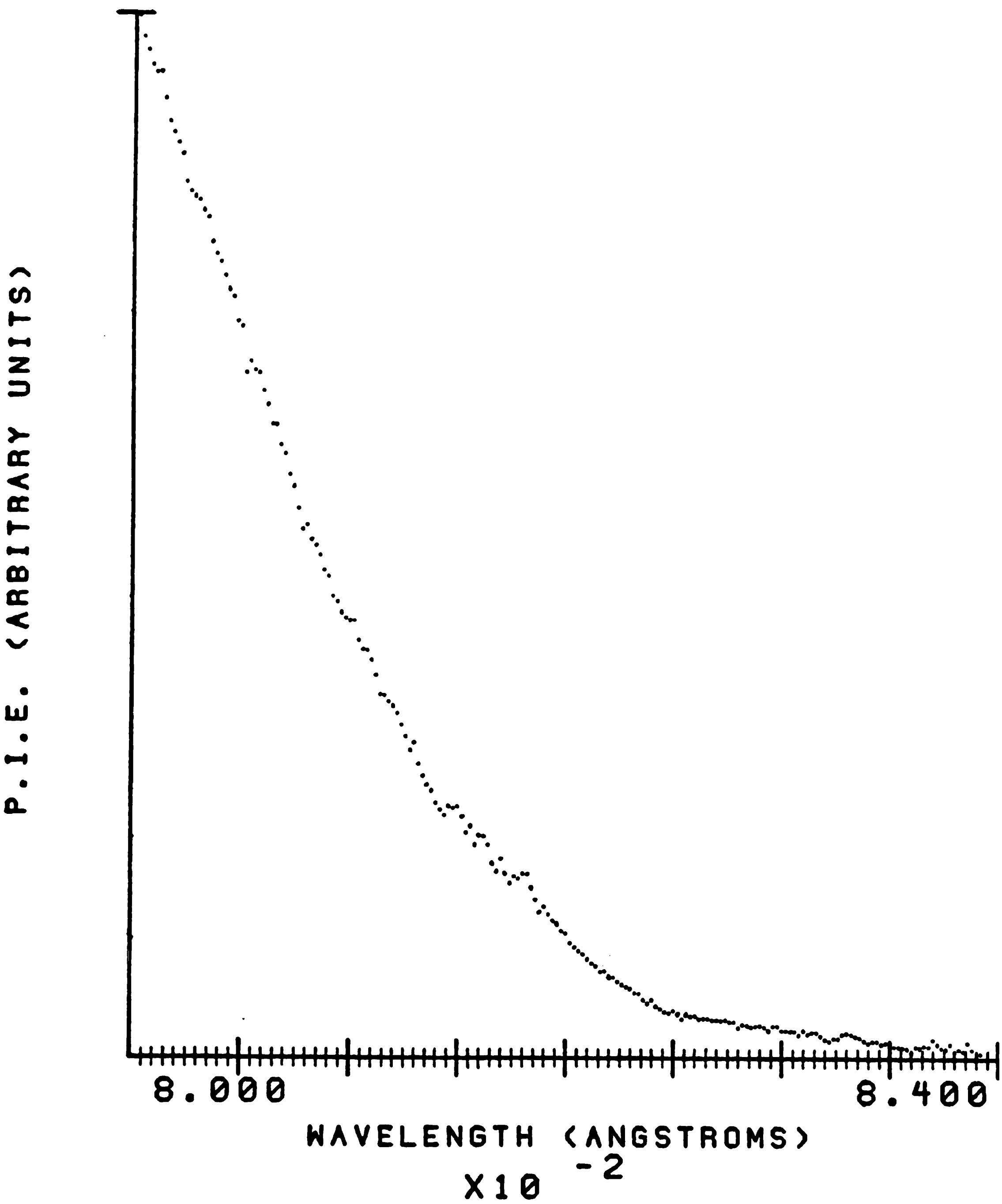
P.I.E. (ARBITRARY UNITS)
8.000
8.400
WAVELENGTH (ANGSTROMS)
X10 -2

effects. Under these circumstances, it is meaningless to extrapolate some portion of the curve to the horizontal axis in order to determine the appearance potential. The best that can be done is to estimate the point at which the low energy tail reaches the horizontal axis. An appearance potential estimated in this way is often an upper bound to the thermodynamic value, because the sensitivity of most instruments is insufficient to detect the increasingly weak signal out to the true threshold. However, given sufficient sensitivity, it is possible to detect ions out to the true threshold - and beyond, if the thermal tail is intense enough. In this case, the measured appearance potential would be a lower bound to the true value. In the present case, the value obtained for the $CH_2^+$ appearance potential is slightly lower than that calculated from the literature[39] (see the next paragraph), indicating that the sensitivity of the MSU PIMS apparatus is sufficient to detect at least a portion of the thermal tail that lies below the threshold energy.

Estimation of the position of the threshold of the $CH_2^+$ P.I.E. curve (Figure III-11) is hampered by the scatter in the data in the low energy tail. The difference between the scatter in the $CH_2^+$ and $CD_2^+$ P.I.E. curves results from the necessity of performing the $CH_2^+$ experiments at twice the mass resolution required for $CD_2^+$. Despite the scatter in the data, it is reasonable to extrapolate the sloping low energy tail to "threshold" at 835.0±1 Å or 14.85 ±0.02 eV. After correction, the 0 °K appearance potential is 832.7±1 Å or 14.89±0.02 eV. This agrees very well with the value of 14.90 eV (Table III-2) which was calculated from the latest thermodynamic literature.[21,39] The value reported here is 0.09 eV lower than the one reported by Dibeler and Liston[23], probably resulting from the difference in sensitivity between the MSU PIMS apparatus and their circa 1968 instrument. When the $CH_2^+$ appearance potential is combined with the 0 °K heats of formation of HCN (1.405 eV)[39] and $H_3CCN$ (0.979 eV)[39], the 0 °K heat of formation of $CH_2^+$ is calculated to be 14.46±0.02 eV or 333.4±0.5 kcal/mol. This is in excellent agreement with the best current literature value of 334 kcal/mol.[21] If Herzberg's value for the ionization potential of $CH_2$ (10.396±0.003 eV)[42] is subtracted from the 0 °K heat of formation of $CH_2^+$, the 0 °K heat of formation of $CH_2$ is calculated to be 4.06±0.02 eV or 93.62±0.5 kcal/mol. This agrees with the current literature value of 93.9 kcal/mol within experimental error.

The threshold region of the $CD_2^+$ P.I.E. curve is quite similar to that of $CH_2^+$ except for some weak structure be tween 815 A and 820 Å. As before, these features are due to inadequately corrected atomic lines and experimental artifacts in the Hopfield continuum. In this case the low energy tail reaches "threshold" at 836.0±1 Å or 14.83±0.02 eV. The corrected value is then 833.8±1 Å or 14.87±0.02 eV.

The proximity of this value to the $CH_2^+$ appearance potential seems reasonable; however, there is no way to give it a valid test due to the lack of thermodynamic data on deuterated species in the literature.

The P.I.E. curve of $CH_2^+$ from threshold to 600 Å (Figure III-13) is quite similar to that of $HCCN^+$. The very shallow slope in the threshold region can be more fully appreciated in this figure. As with $HCCN^+$, the P.I.E. curve does not begin to rise sharply until the region of the threshold of the parent ion $\overline{B}^2E$ state is reached (approximately 820 Å). Once again, predissociation of this state must contribute strongly to the formation of this ion.

$\underline{CH_3^+ \text{ and } CD_3^+}$

The $CH_3^+$ P.I.E. curve from threshold to 600 Å is presented in Figure III-14. It has not been previously reported in the open literature. Due to the extremely weak ion signal, the P.I.E. curve was measured with an electron multiplier as the photon transducer. The overall curve has been approximately corrected for the wavelength dependence of the multiplier's sensitivity. Despite this, its similarity to the $HCCN^+$ and $CH_2^+$ P.I.E. curves is easily discerned. The low energy tail in the threshold region is not as pronounced as that of $CH_2^+$. This might be expected as the formation of $CH_3^+$ and CN is likely to be a more direct process than the formation of $CH_2^+$ and HCN, which

Figure III-13. The $CH_2^+$ P.I.E. curve from threshold to 600 Å.

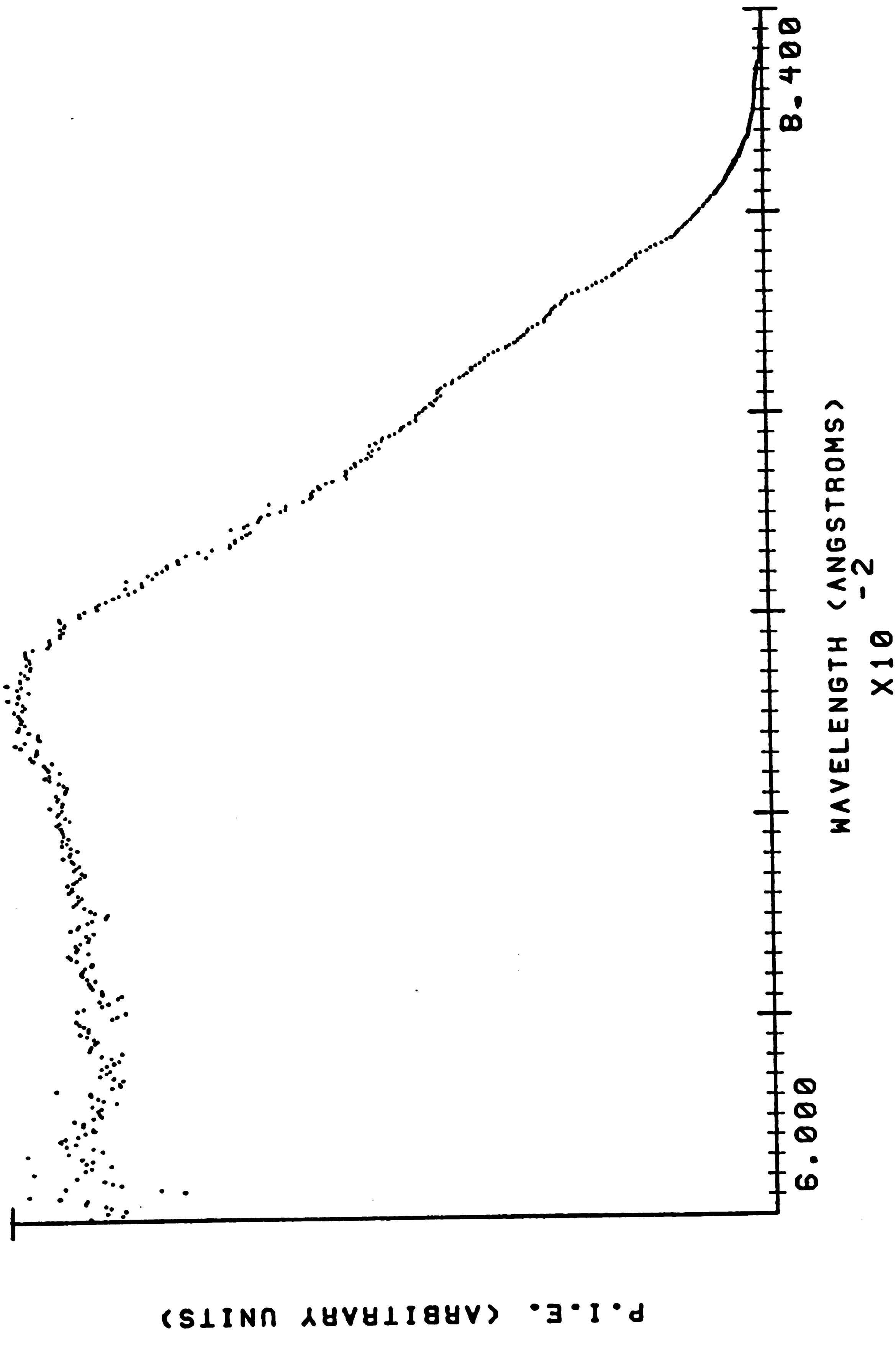
8.400
6.000
WAVELENGTH (ANGSTROMS)
X10^-2
P.I.E. (ARBITRARY UNITS)

Figure III-14. Threshold region of the $CH_3^+$ P.I.E. curve.

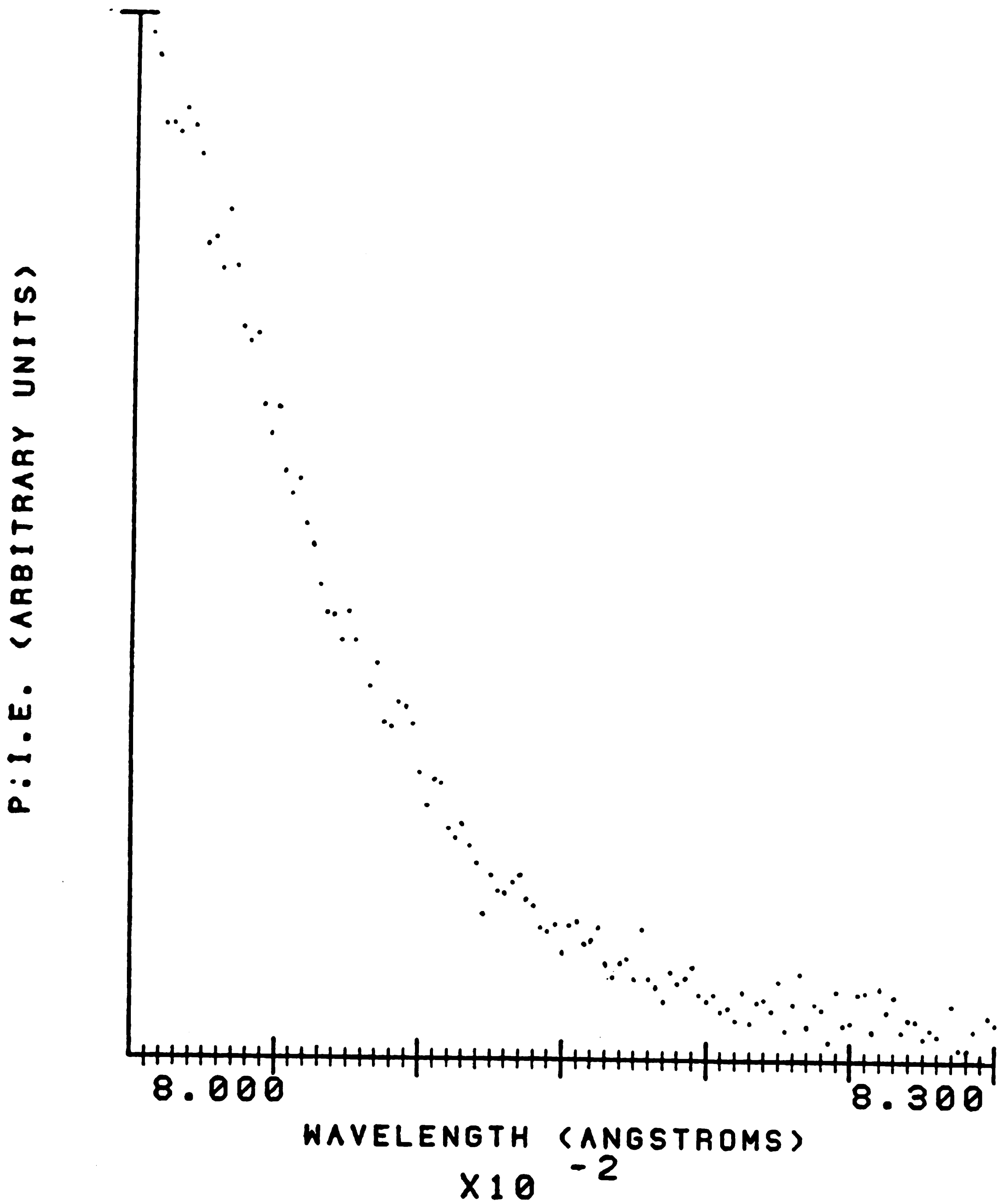
P.I.E. (ARBITRARY UNITS)
8.000
8.300
WAVELENGTH (ANGSTROMS)
X10 -2

requires the transfer of one of the acetonitrile methyl group hydrogen atoms. As with the fragment ions discussed earlier, the curve does not increase sharply until after the threshold of the parent ion's $\tilde{B}^2E$ state. Thus, predissociation of this state seems to play a major role in the formation of all the fragment ions studied here.

The threshold of the $CH_3^+$ P.I.E. curve (Figure III-15) appears to level-off at 821.5±1 Å or 15.09±0.02 eV. Corrected for the average thermal energy available at 300 °K, the 0 °K $CH_3^+$ appearance potential is 819.5±1 Å or 15.13 ±0.02 eV. From this datum and the 0 °K heats of formation of $H_3CCN$ (0.979 eV)[39] and CN (4.58±0.1 eV)[45] the 0 °K heat of formation of $CH_3^+$ is found to be 11.53±0.1 eV or 265.9±2 kcal/mol. This differs from the current literature value (262 kcal/mol)[39] by more than the experimental error. Since the literature value is based in part on Herzberg's value for the ionization potential of $CH_3$ (9.842 ±0.003 eV)[25], it should be fairly reliable. This would indicate that either the $CH_3^+$ appearance potential reported here is too high or the CN heat of formation reported by Berkowitz, Chupka and Walter[45] is too low. The $CH_3^+$ appearance potential calculated from the $CH_3^+$ and CN heats of formation in the literature[39,45] is 828.9 Å or 14.96 eV. This thermodynamic check, plus the sloping nature of the $CH_3^+$ appearance potential and the scatter in the data suggest that the $CH_3^+$ appearance potential measured in

Figure III-15. Threshold region of the $CD_3^+$ P.I.E. curve.

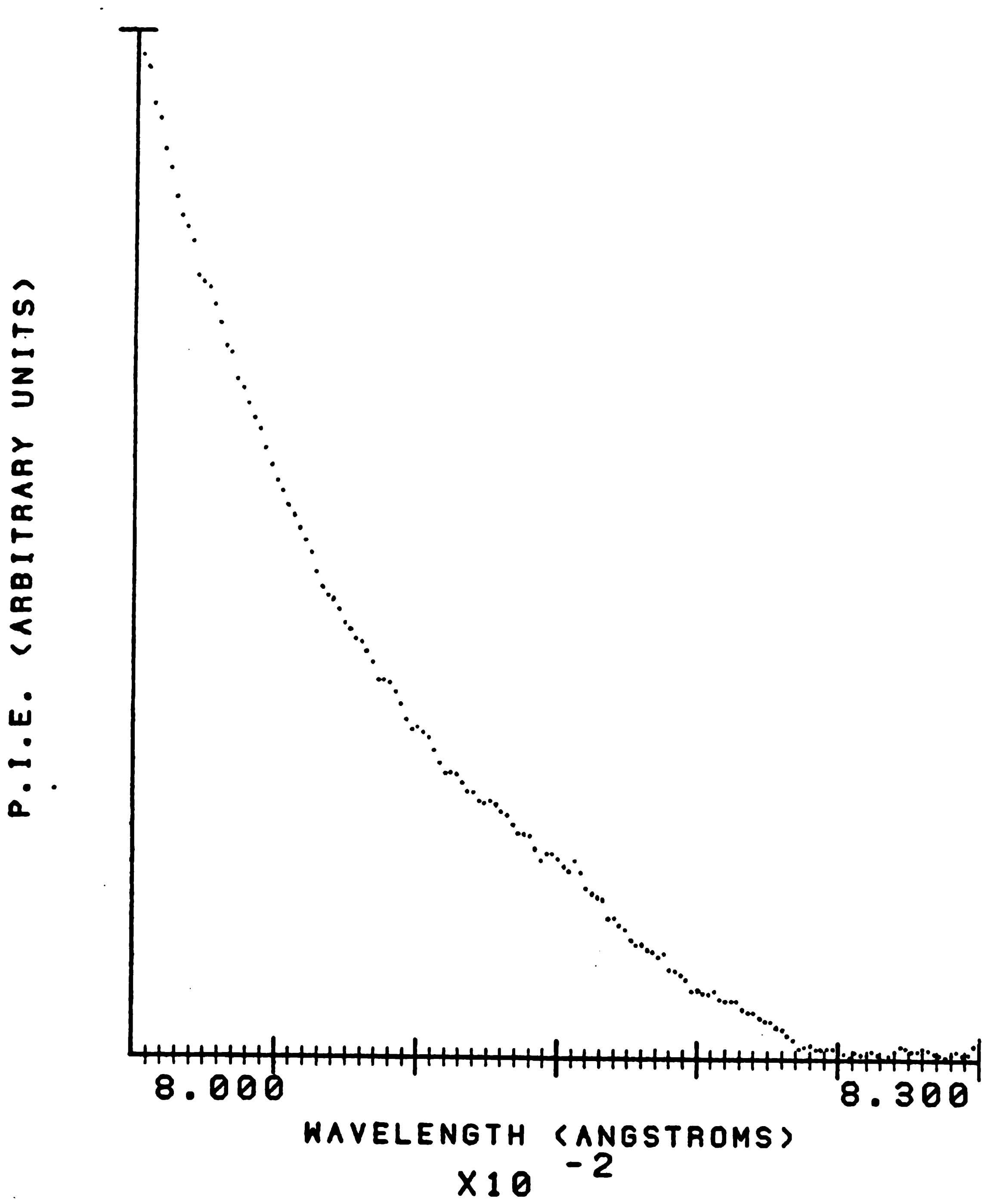
P.I.E. (ARBITRARY UNITS)
8.000
8.300
WAVELENGTH (ANGSTROMS)
X10 -2

this work is too high. It is interesting to note that the value of $D_0(H_3C\text{-}CN)$, 5.29±0.02 eV, calculated by subtracting the ionization potential of $CH_3$[25] from the $CH_3^+$ appearance potential reported here is equal within experimental error to the $D_0(H_3C\text{-}CN)$ reported by Okabe and Dibeler (5.32 ±0.03 eV) from flash photolysis experiments.[24] Thus, it appears that their value may be high as well.

The threshold of the $CD_3^+$ P.I.E. curve (Figure III-16) also has a shallow slope. The curve reaches the horizontal axis at 823.5±0.5 Å or 15.06±0.01 eV. When corrected for the average rotational energy at 300 °K and the photon beam half-width, the $CD_3^+$ 0 °K appearance potential is 821.0±0.5 Å or 15.10±0.01 eV. The thermodynamic data required to test this determination or for the derivation of further parameters are unavailable.

## C. Summary

In summary, the complete P.I.E. curves of $H_3CCN^+$, $H_2CCN^+$, $HCCN^+$, $CH_2^+$, $CH_3^+$ and $D_3CCN^+$ resulting from the photoionization of acetonitrile and acetonitrile-$d_3$ have been determined for the first time. Their appearance potentials have been determined and also those of $D_2CCN^+$, $DCCN^+$, $CD_2^+$ and $CD_3^+$. The appearance potentials of the deuterated ions as well as that of $CH_3^+$ have not been reported heretofore. An autoionizing Rydberg series has been observed in the P.I.E. curves of $H_3CCN^+$ and $D_3CCN^+$

Figure III-16. The $CH_3^+$ P.I.E. curve from the threshold to 600 Å.

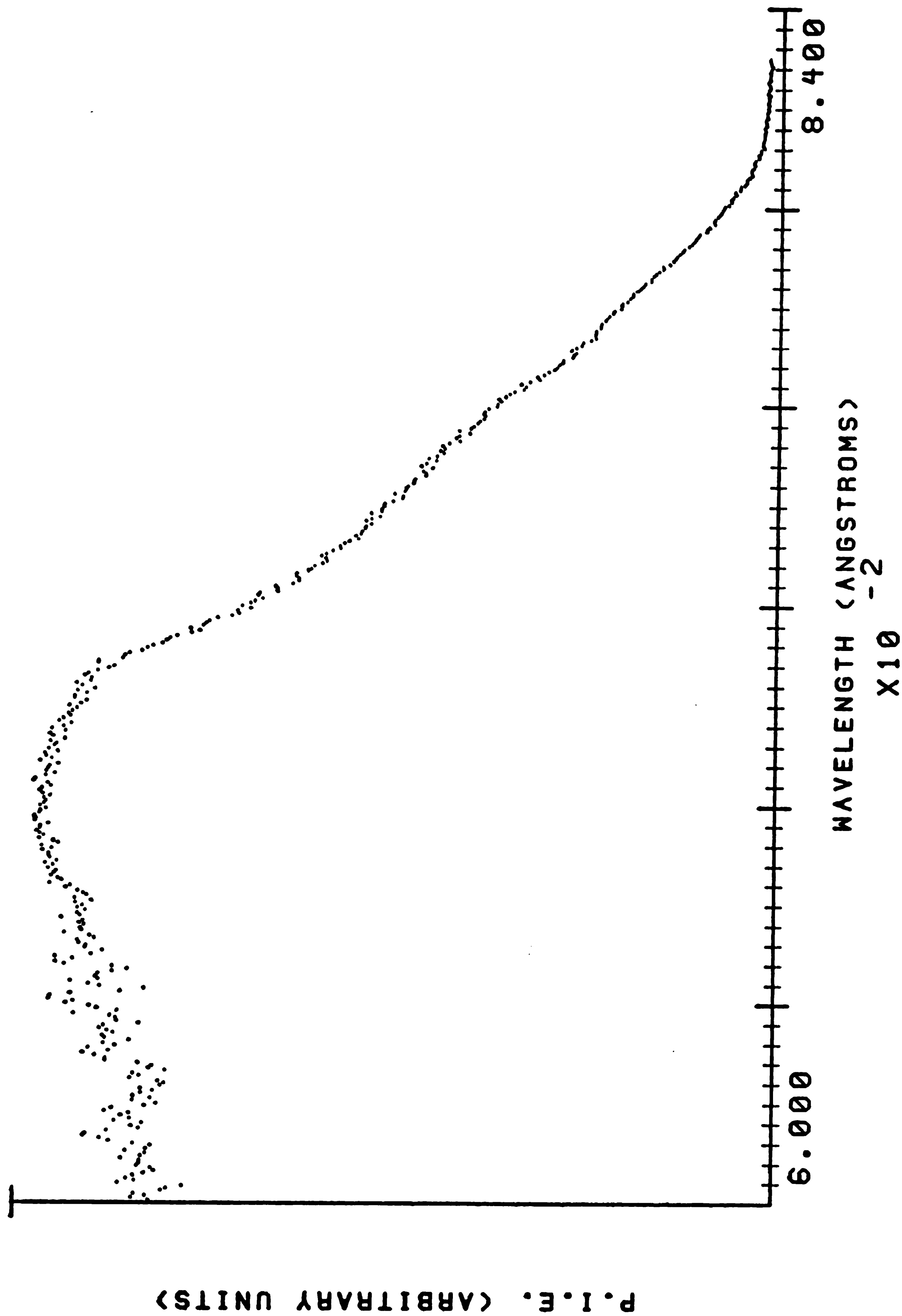
8.400
6.000
WAVELENGTH (ANGSTROMS)
X10 -2
P.I.E. (ARBITRARY UNITS)

and assigned as an ns$\sigma$ series converging to the $\bar{A}^2A_1$ state of the parent ion. All of the fragment ions studied have appearance potentials that lie between the thresholds of the $\bar{A}^2A_1$ and $\bar{B}^2E$ states of the parent ions. At lower energies they appear to be formed by the predissociation of autoionizing Rydberg states. However, after the energy of the exciting light has reached the threshold of the $\bar{B}^2E$ state of the parent ion (15.13 eV or 819.5 Å), the fragment ion P.I.E. curves rise sharply, indicating that most of their intensity is the result of the predissociation of this state. Finally, the appearance potentials reported here have been used to derive several thermodynamic parameters. These results are summarized in Table III-7.

Table III-6. Appearance potentials of the fragment ions of $H_3CCN^+$ and $D_3CCN^+$ corrected to 0 °K.

| Ion | Neutral Fragment | Appearance Potential |
|---|---|---|
| $H_2CCN^+$ | H | 14.047±0.006 eV |
| $D_2CCN^+$ | D | 14.05±0.01 eV |
| $HCCN^+$ | $H_2$ | 15.15±0.01 eV |
| $DCCN^+$ | $D_2$ | 15.10±0.05 eV |
| $CH_2^+$ | HCN | 14.89±0.02 eV |
| $CD_2^+$ | DCN | 14.87±0.02 eV |
| $CH_3^+$ | CN | 15.13±0.02 eV |
| $CD_3$ | CN | 15.10±0.01 eV |

Table III-7. Derived thermodynamic quantities.

| Ion | Thermodynamic Quantity |
|---|---|
| $H_2CCN^+$ | $\Delta H^{\circ}_{f_0}$ $(H_2CCN^+)$ = 12.787±0.006 eV (294.88±0.15 kcal/mol) |
| | $\Delta H^{\circ}_{f_0}$ $(H_2CCN)$ = 1.92±0.1 eV (44.4±2 kcal/mol) |
| | $D_0$ $(H{-}CH_2CN)$ = 3.18±0.1 eV (73.5±1 kcal/mol) |
| $HCCN^+$ | $\Delta H^{\circ}_{f_0}$ $(HCCN^+)$ = 16.13±0.01 eV (372±0.2 kcal/mol) |
| $CH_2^+$ | $\Delta H^{\circ}_{f_0}$ $(CH_2^+)$ = 14.46±0.02 eV (333.4±0.5 kcal/mol) |
| | $\Delta H^{\circ}_{f_0}$ $(CH_2)$ = 4.06±0.02 eV (93.62±0.5 kcal/mol) |
| $CH_3^+$ | $\Delta H^{\circ}_{f_0}$ $(CH_3^+)$ = 11.53±0.1 eV (265.9±2 kcal/mol) |
| | $D_0$ $(H_3C{-}CN)$ = 5.29±0.02 eV (121.99±0.5 kcal/mol) |

# REFERENCES

## REFERENCES


1. Turner, Barry E., Scientific American, 228, 50 (1973).

2. Gordon, M. A. and Snyder, L. E., Molecules in the Galactic Environment, Wiley-Interscience, New York, 1973.

3. Solomon, Philip M., Physics Today, 26(3), 32 (1973).

4. Herbst, Eric and Klemperer, William, Physics Today 29(6), 32 (1976).

5a. Chupka, W. A., "Ion-Molecule Reactions by Photoionization Techniques", in Ion-Molecule Reactions, Vol. I, J. L. Franklin, Ed., Plenum Press, New York, pp. 33-76 (1972).

5b. Chupka, W. A., "Photoionization and Fragmentation of Polyatomic Molecules", in Chemical Spectroscopy and Photochemistry in the Vacuum Ultraviolet, Sandorfy, C., Ausloos, P. J. and Robin, M. B., D. Reidel Publishing Co., pp. 431-463 (1974).

5c. Chupka, W. A., "Effects of Internal Energy Effects on Ion-Molecule Reactions", in Interaction Between Ions and Molecules, Ausloos, P. J., Ed., Plenum Press, New York, pp. 249-262 (1975).

6. Reid, N. W., Int. J. Mass Spectrom. Ion Phys. 6, 1 (1971).

7. Samson, J. A. R., Sci. Tech. Aerosp. Rep. 14(12), (1976).

8. Nicholson, A. J. C., J. Chem. Phys. 39, 954 (1963).

9. Wigner, E., Phys. Rev. 73, 1002 (1948).

10. Chupka, W. A., Berkowitz, J. and Rafaey, K. M. A., J. Chem. Phys. 50(5), 1938 (1969).

11. Duncan, A. B. F., Rydberg Series in Atoms and Molecules, Academic Press, New York, 1971.

12. Fano, U. and Cooper, J. W., Rev. Mod. Phys. 40, 441 (1968).

13. Chupka, W. A., J. Chem. Phys. 10(1), 191 (1959).

14. Chupka, W. A., J. Chem. Phys. 54(5), 1936 (1971).

15. Robin, M. B., Higher Excited States of Polyatomic Molecules, Vol. II, Academic Press, New York, p. 292 (1974).

16. Darland, E. J., Doctoral Dissertation, Michigan State University, 1977.

17. Buttrill, S. E., Jr., J. Chem. Phys. 61(1), 619 (1974).

18. Williamson, A. D., Doctoral Dissertation, California Institute of Technology, 1975.

19. Samson, J. A. R., Techniques of Vacuum Ultraviolet Spectroscopy, John Wiley and Sons, New York, 1967.

20. Franklin, J. L., Wada, Y., Natalis, P. and Heirl, P. M., J. Phys. Chem. 70, 2353 (1966).

21. Energetics of Gaseous Ions, in J. Phys. Chem. Ref. Data 6(1), Rosenstock, H. M., Draxl, K., Steiner, B. W., and Herron, J. T., Editors, 1977.

22. Haney, Max and Franklin, J. L., J. Phys. Chem. 73(12), 4328 (1969).

23. Dibeler, V. H. and Liston, S. K., J. Chem. Phys. 48, 4765 (1968).

24. Okabe, H. and Dibeler, V. H., J. Chem. Phys. 59, 2430 (1973).

25. Herzberg, G. and Shoosmith, J., Can. J. Phys. 34, 523 (1956).

26. Binding Energies in Atomic Negative Ions, in J. Phys. Chem. Ref. Data 4(3) Hotop, H. and Lineberger, W. C., Editors, 539 (1976).

27. Watanabe, K., Nakayama, T. and Mottl, J., J. Quant. Spectry. Radiative Transfer 2, 369 (1962).

28. Nicholson, A. J. C., J. Chem. Phys. 43, 1171 (1905).

29. Lake, R. F. and Thompson, H., Proc. Roy. Soc. Lond. A. 317, 187 (1970).

30. Frost, D. C., Herring, F. G., McDowell, C. A. and Stenhouse, I. A., Phys. Letters 4, 533 (1970).

31. Turner, D. W., Baker, C., Baker, A. D. and Brundle, C. R., Molecular Photoelectron Spectroscopy, Wiley-Interscience, London, 1970.

32. Guyon, P. M. and Berkowitz, J., J. Chem. Phys. 54 (4), 1814 (1971).

33. Yee, D. S. C. and Brion, C. E., J. Electron Spec. and Rel. Phenomena 8, 313 (1976).

34. Baybritt, P., Guest, M. F. and Hillier, I. H., Mol. Phys. 25(5), 1025 (1973).

35. Shimanouchi, T., Tables of Molecular Vibrational Frequencies, Consolidated Volume I, NSRDS-NBS 39, 84 (1972).

36. Cutler, J. A., J. Chem. Phys. 16(2), 136 (1948).

37. Stradling, R. S. and Loudon, A. G., JCFTBS 73(5), 623 (1977).

38. Dibeler, B. H., Walker, J. A., McCulloh, K. E. and Rosenstock, H. M., Int. J. Mass Spectrom. Ion Phys. 7, 209 (1971).

39. Wagman, D. D., Evans, W. H., Parker, V. B., Halow, I., Bailey, S. M. and Schumm, R. H., NBS Tech. Note 270-3 (U.S. Government Printing Office, Washington, D.C., 1968).

40. Pottie, R. F. and Lossing, F. P., J. Am. Chem. Soc., 83, 4737 (1961).

41. Haney, M. A. and Franklin, J. L., J. Chem. Phys. 48 (9), 4093 (1968).

42. Guyon, P. M., Chupka, W. A. and Berkowitz, J., J. Chem. Phys. 64(4), 1419 (1976).

43. Chupka, W. A., J. Chem. Phys. 48, 2337 (1968).

44. Herzberg, G., Can. J. Phys. 39, 1511 (1961).

45. Berkowitz, J., Chupka, W. A. and Walter, T. A., J. Chem. Phys. 50(4), 1497 (1969).

46. McCulloh, K. E. and Dibeler, V. H., J. Chem. Phys. 64(11), 4445 (1976).